Degree Thesis for Doctor of Philosophy

A Study on the Phase-asynchronous PD Diagnosis Method

for Gas Insulated Switchgears

Supervisor : Prof. Gyung-Suk Kil

August 2017

Department of Electrical and Electronics Engineering

The Graduate School of Korea Maritime and Ocean University

Sung-Wook Kim

Thesis submitted by Sung-Wook Kim in Fulfillment

of Requirement for the Degree of Doctor of Philosophy

Committee Chairman : D. Eng. Yoon-Sik Kim ㊞

Committee Member : D. Eng. Gyung-Suk Kil ㊞

Committee Member : D. Eng. Nak-Won Jang ㊞

Committee Member : D. Eng. Heung-Gi Cho ㊞

Committee Member : D. Eng. Young-Jin Cho ㊞

August 2017

Department of Electrical and Electronics Engineering

The Graduate School of Korea Maritime and Ocean University

Sung-Wook Kim

Contents

Lists of Figures and Tables

\<List of Figures\>

\<List of Table\>

A Study on the Phase-asynchronous PD Diagnosis Method

for Gas Insulated Switchgears

by Sung-Wook Kim

Department of Electrical and Electronics Engineering

The Graduate School of Korea Maritime and Ocean University

Busan, Republic of Korea

Abstract

Gas-insulated switchgear (GIS) is one of the most important power facilities and a valuable asset in a power system for providing stable and reliable electrical power. It has been in operation for more than 45 years due to its high reliability with low failure rate. Although GIS has a low-maintenance requirement, its failure caused by partial discharge (PD) leads to considerable financial loss.

The ultra-high frequency (UHF) method is an effective tool to detect insulation defects inside GIS and widely used for on-line and on-site diagnosis. It is also less sensitive to noise as well as better for PD detection compared to other measurement methods. Most of utilities, laboratories, and countries perform the PD detection using narrow-band or wide-band frequency

ranges and classify types of PDs by conventional methods with a phase angle of the voltage applied to power equipment. In many cases of on-site PD measurement in the field, however, it is difficult to classify types of PDs due to the phase-asynchronous PD signals.

This thesis described a new method of PD diagnosis which can classify types of PDs without phase information of the voltage applied to GIS. The 327 cases of on-site measurement data were collected from 2003 to 2015. The statistical analysis of collected on-site measurement data was performed according to voltage classes, maintenance results, defect causes, and defect locations. From the statistical analysis, the most frequent PD and noise types were a floating element and an external interference, respectively.

To develop the new method of PD diagnosis which is applicable to the on-site PD diagnosis without phase synchronization, the features were extracted to classify defect types using the representative data of 82 cases, including 66 PD and 16 noise cases. The features consisted of 5 frequency and 6 phase parameters. The 5 frequency parameters were the number of distribution ranges, maximum value, ranges of first and second peak value, peak differences between first and second peak value, and density levels. 6 phase parameters were the number of phase groups, overall distribution ranges or not, the distribution ranges of each group, density levels, peak differences between first and second group, and shapes. 82 cases of representative data were selected through the review of data validation and analyzed using the designed 11 feature parameters, from which 5 effective parameters were extracted to identify the defect types using the decision tree-based technique by 4 steps: the number of groups in phase parameters (first step), shapes in

phase parameters (second step), the number of distribution ranges & density levels in frequency parameters (third step), and ranges of first and second peak value in frequency parameters (fourth step). As a result, the decision tree-based diagnosis algorithm was able to classify types of 6 PDs and 4 noises and 77 of 82 cases were exactly classified. The diagnosis performance of new method proposed in this thesis therefore had an accuracy rate over 94% and was able to diagnose almost every type of defect.

The new method also was applied to on-site GIS diagnosis in South Korea and Malaysia to verify its reliability. In two cases, portable and on-line UHF PD systems were installed without phase synchronization, and the defect cause and location inside GISs were inspected visually by on-site engineers after on-site PD measurement. The two cases were analyzed by the new method based on decision-tree based diagnosis algorithm and results of the new method were identical to results of internal inspection. From the results, the new method of PD diagnosis proposed in this thesis is quite useful to classify various defect types using the phase-asynchronous PD signals in the on-site measurement.

Chapter 1 Introduction

Gas-insulated switchgear (GIS) is widely applied to power system since 1960s and is one of the important power facilities and a valuable asset for providing stable electrical power. A GIS consists of a bushing, a circuit breaker, a voltage and current transformer, a lightning arrester, and other components in Fig. 1.1. SF_6 gas used as an insulating medium in GIS has excellent dielectric and arc-quenching property. Therefore, the GIS has been in operation for more than 45 years due to its high level of reliability with very low failure rates[1],[2]. However, insulation accidents of GIS occur yearly because the construction of power system is more complicated and fault current and transient voltage are more severe as well as insulation distance is shortened by reducing GIS size while the capacity of power system increases.
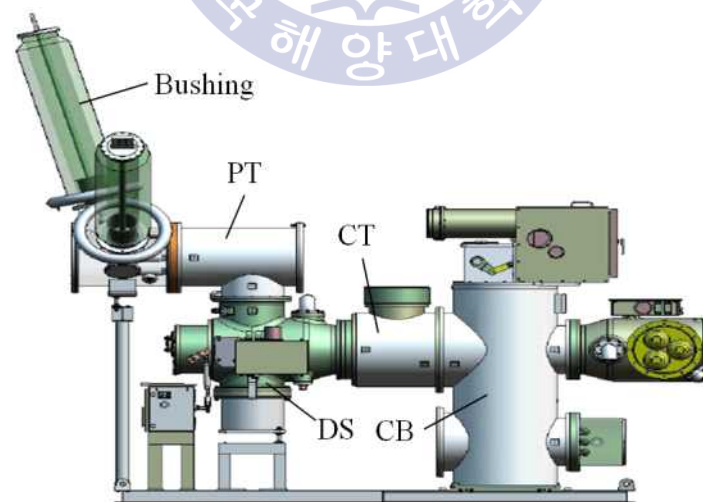
Fig. 1.1 Configuration of a GIS

Fig. 1.2 shows GIS major failure frequencies (MaF) in GISs for manufacturing year intervals and voltage classes investigated until 2007 from CIGRE working group A3.06 in 2012. The 24 countries and 55 utilities took part in the survey with an average total population of about 22,240 GIS-bays. The collected GIS's service experience of 88,971 circuit breaker-bay-years (CB-bay-years) had 358 major failures. It showed the MaF of 0.37 per 100 GIS CB-bay-years with all data. The MaF frequency was higher 3 times than the target failure rate recommended in IEC 60071-2, which is 0.1 MaF frequency per 100 bay-years for GIS insulation coordination[3]-[5].

	2007-2004	2003-1999	1998-1994	1993-1989	1988-1984	1983-1979	before1979
■ $60 \leq U < 100kV$	0.40	0.08	0.20	0.27	0.50	0.39	0.51
■ $100 \leq U < 200kV$	0.33	0.08	0.13	0.11	0.64	1.29	1.98
■ $200 \leq U < 300kV$	0.22	0.40	0.46	0.49	0.13	0.14	0.14
■ $300 \leq U < 500kV$	0.58	0.31	0.34	0.61	1.36	1.99	4.05
■ $500 \leq U < 700kV$	0.00	0.19	0.58	0.39	0.00	1.39	0.00
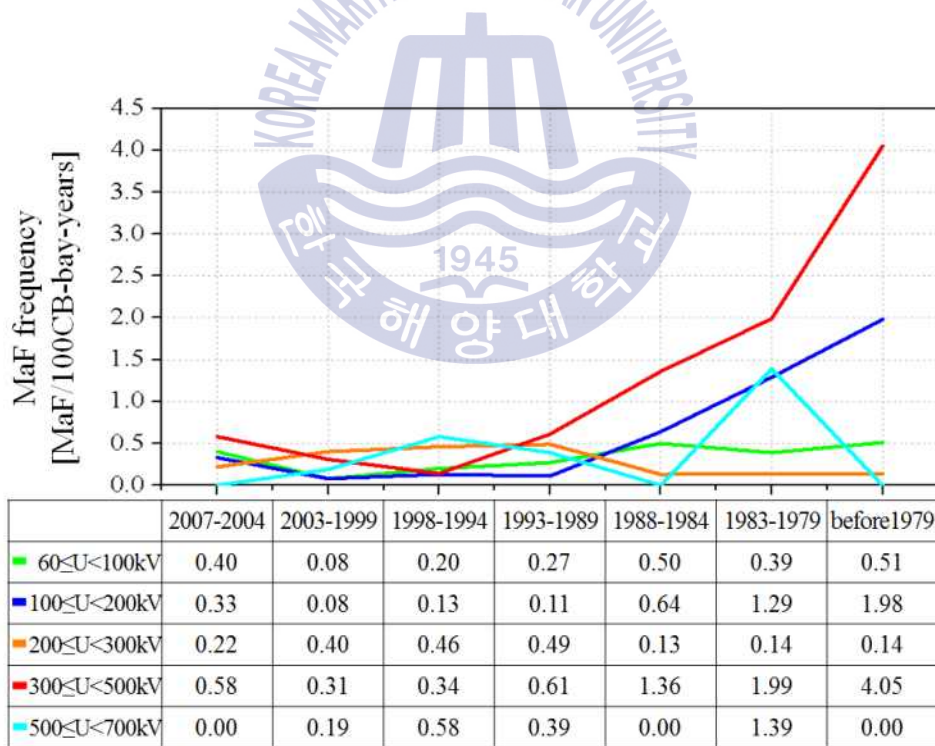
Fig. 1.2 Major failure frequencies in GISs

When GIS fails by deterioration, it may cause a significant economic loss because the high-capacity power system has been expanded to meet the rapid increase of electrical power usage. Therefore, there has been increasing interest in reliable power supply and integrity evaluation of power facilities[6]-[8]. Traditionally, the maintenance strategy for electrical equipment was based on fixed intervals or the number of operations; this is called time-based maintenance (TBM). More recently, the strategy has evolved to condition-based maintenance (CBM), which can monitor equipment conditions in real time. In particular, the GIS condition monitoring and diagnosis technique for preventing insulation breakdown are more important because of the high power supplied by each unit[9].

The worldwide in-service return of experience for GIS is presented in Fig. 1.3. About 30% of the dielectric failures are related to design deficiencies. Other failures are related to quality assurance problems. Failures caused by mobile particles represent 20% of the total number. Loose shields lead to floating element type defects while current carrying contacts create galling type defects; both of them are common malfunctions. Problems related to insulators surface contamination by particles and voids in the bulk insulation cannot be excluded[10],[11].
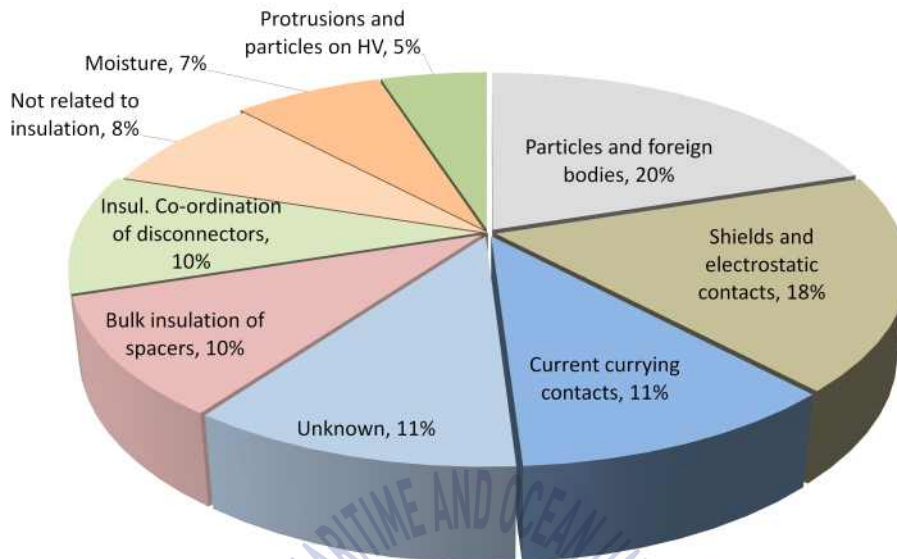
Fig. 1.3 Mean distribution of dielectric failure in service

The GIS diagnosis techniques are classified into SF_6 gas decomposition, gas leakage, vibration, partial discharge (PD), and others. One of the major techniques for GIS is PD diagnosis method and it is widely used to detect insulation deterioration and to identify defect types of GIS. Technical methods for PD diagnosis are composed of a conventional method based on IEC 60270 and non-conventional methods including ultra-high frequency (UHF) and acoustic emission (AE) method. Especially, the UHF method detects electromagnetic signals emitted from PD sources with a frequency range from 0.3 to 3 GHz and it is an effective tool to detect insulation defects related to over 50 percent of GIS failures[12]-[14]. Most of utilities, laboratories, and countries use the UHF method for on-line and on-site diagnosis because it is less sensitive to noise as well as better for PD detection compared to other

measurement methods.

Classifying types of defects in GIS are very important to reduce time and cost of on-site maintenance work. The typical PDs occurring inside GIS are free moving particle, protrusion fixed on the enclosure and conductor, floating metallic parts as well as cavities due to voids and cracks in spacers. There are classic PD analysis methods for the classification of PD types, such as phase resolved partial discharge (PRPD), frequency and phase spectrum, and T-F map[15]-[18]. Some of them, the PRPD method as well as the phase spectrum analysis method use the discharge phase to analyze PD patterns. The discharge phase is one of the important parameters, especially with respect to PD classification, and it is necessary to have PD signals synchronized with the phase of voltage applied to GIS in the field since the result of PD diagnosis is strongly influenced by zero crossing of phases angle between PD signals and the applied voltage. However, the users avoid using the potential transformer (PT) signal from energized GIS which can measure the phase of voltage applied to the GIS. It is also impossible to classify PD types in three-phase construction. Thus, precise and reliable PD diagnosis cannot be performed in many cases of on-site PD measurement. Therefore, a new method of PD diagnosis applicable without phase information might be considered since the phase-asynchronous PD pattern often gives an incorrect diagnosis.

This thesis dealt with the new method of PD diagnosis which can classify the types of PDs without phase information. The cases of on-site measurement data were collected for over 10 years including measuring data and time, frequency and phase spectrum of PD signals, diagnosis result,

defect cause, defect location, and other information, visually inspected by experienced engineers and maintenance experts. The statistical analysis of collected on-site measurement data was performed according to voltage classes, maintenance results, defect causes, and defect locations.

The features were defined to classify types of defects; frequency parameters were the number of distribution ranges, maximum values, ranges of first and second peak value, peak differences between first and second peak value, and density levels; phase parameters were the number of groups, overall distribution ranges or not, distribution ranges of each group, density levels, peak differences between first and second group, and shapes. Using representative data, effective parameters of them were extracted to classify types of 6 PDs and 4 noises clearly.

The new algorithm was designed by 5 effective parameters using the decision tree method. The decision tree-based diagnosis algorithm can classify types of PDs and noises by 4 steps: the number of groups in phase parameters, shapes in phase parameters, the number of distribution ranges & density levels in frequency parameters, and ranges of first and second peak value in frequency parameters.

To evaluate the new PD diagnosis method proposed in this thesis, 82 cases of representative data were used to compare the diagnosis performance between the new method and the conventional method. The new method was also applied to on-site GIS diagnosis in South Korea and Malaysia to verify its reliability. In two cases, portable and on-line UHF PD systems were installed without phase synchronization, and the defect cause and location inside GIS were inspected visually by on-site engineers.

From the result, the new method of PD diagnosis is able to classify types of PDs and noises clearly. As the phase-asynchronous PD data were collected from the UHF sensors and the PD analyzers installed on the GISs managed by Hyosung corporation, the diagnosis performance of new method thus applies only to these types of PDs and noises. After comprehensive analysis, it is expected that the new method can be applied to other power facilities such as high-voltage transformers, motors, gas-insulated transmission line (GIL), as well as GISs designed by other manufacturers.

Chapter 2 Partial Discharges

PD occurs due to the created space charge and it depends on the local field strength in the vicinity of defects and on the type of the applied voltage, such as continuous AC and DC voltages as well as transient switching and lightning impulse voltage[19]. In IEC 60270, a PD is defined as a localized electrical discharge that only partially bridges the insulation between conductors and which can or cannot occur adjacent to a conductor. PD activity can occur at any point in the insulation system, where the electric field strength exceeds the breakdown strength of that portion of the insulating material. Although the magnitude of such discharge is usually small at its early stage, it causes progressive deterioration and finally results in the failure of power apparatus such as power transformer, GIS, and GIL. It is therefore essential to detect PD for condition monitoring and diagnosis of the insulation system[12],[20].

2.1 PD Classification

To diagnose the degree of insulation deterioration, it is necessary to measure an accurate PD signal and to distinguish whether occurring PD source is generated inside the insulation or not. PDs can be classified into external discharge, surface discharge, and internal discharge. The external discharge is generally called corona discharge and it is an electrical discharge formed by the ionization of a fluid such as air surrounding a conductor that is electrically charged as shown in Fig. 2.1. When the applied voltage is

Collection @ kmou

closed to the inception voltage, glow and streamer discharges appear. Stable leader discharge only occurs in very long air gaps. Although chemical processes are excited by gas discharges, the created by-products are continuously substituted by the circulating gas. Therefore, discharge processes in pure ambient air can be considered as reversible and thus as harmless in general. External discharges, however, in ambient air propagating along solid dielectric surface become harmful because they create irreversible degradation processes[19].
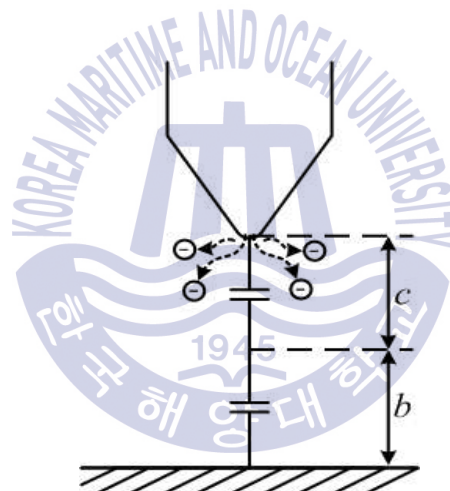
Fig. 2.1 Corona discharges

The discharge starts when free electrons in air are accelerated by the electric field. The electrons with enough energy by the electric field generate ions by colliding atoms and thereby ionize them. This process releases additional electrons which accelerate and collide with further atoms, and more electrons are released. The initial electrons are formed by photoelectrons. The process of electron avalanche is shown in Fig. 2.2[21],[22].

(a) Inception
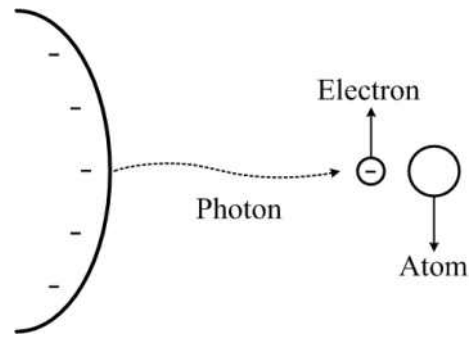
(b) Electron formation
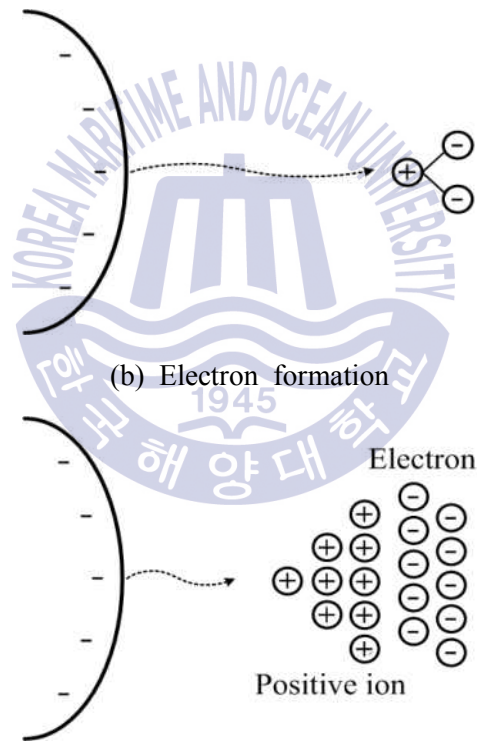
(c) Electron avalanche

Fig. 2.2 Process of an electron avalanche

In this process, an electron is expelled from the molecule (M) during the collision process to convert the molecule to a positive ion with an odd

number of electrons[22]. The electron ionization process is equal to:

$$M + e \rightarrow M^+ + e + e \qquad (2.1)$$
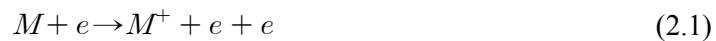
where M is the molecule being ionized, e is the electron, and M^+ is the resulting molecular ion.

When free electrons accelerated by an electrical field collide with medium's atoms and additional electrons are generated. The number of electrons increases rapidly in this process, which is called an electron avalanche. The current flowing in the electron avalanche is equal to:

$$I = I_0 e^{\alpha d} \qquad (2.2)$$

where d is the distance between the electrodes and a is the first Townsend ionization coefficient.

The first ionization coefficient represents the number of electrons generated by a negative ion moving per a length of 1 cm and the amount of electrons increase, which is called primary process. After primary process, the positive ions and photons collide with electrodes and more electrons are released, which is called secondary process. The electrons released though primary and secondary processes are absorbed depending on the polarity of electrodes or attached to medium's atoms to create negative ions. A corona discharge occurs when the strength of local electric field is high enough on a conductive region, but not enough to cause insulation breakdown in other regions. The corona occurs at the portion where the electrical field is

concentrated over the critical electric field of E_o.

$$E_o = 30 \ \delta M \qquad (2.3)$$

where E_0 is electric field strength of corona inception, δ is the relative air density, P is the air pressure, θ is the temperature, and M is surface coefficient of conductor.

Surface discharges are caused by the short leakage distance due to deficiencies of insulation design and the reduction of effective leakage distance due to the surface contamination. Fig. 2.3 shows the occurrence of a surface discharge. It may not affect the deterioration of the insulating system at an early stage but the high-frequency voltage generated by the surface discharge is overlapped with the AC voltage, which causes excessive
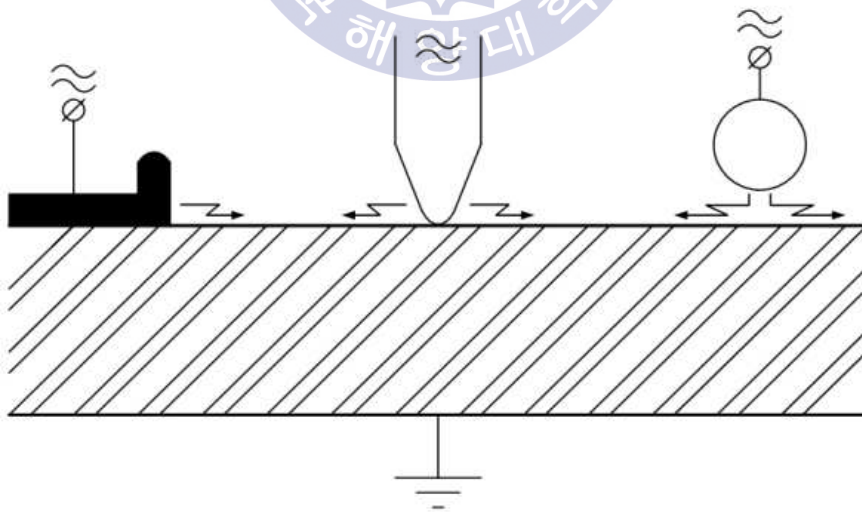
Fig. 2.3 Surface discharges

electrical stress, thereby damaging the insulation. If the surface discharges occur for a long period of time, the deterioration is concentrated on the defective portion of insulating material and the electrical and mechanical properties of insulating system are damaged. When the deterioration further proceeds, carbonized conductive path is formed and it leads to insulation breakdown[23].

Internal discharges occur in gas-filled cavities such as voids, cracks or even in defects of the molecular structure under low dielectric strength. Especially, the occurrence of voids significantly deteriorates the performance of insulating material and reduces the life of the power facilities. In Fig. 2.4, when the void occurs inside the solid insulator and high voltage is applied to the solid insulator, the electric field is concentrated inside the void because dielectric constant of the void is lower than that of the solid insulator. Finally, gas discharge occurs due to low dielectric strength of gas inside the void.

In Fig. 2.5, the equivalent circuit represents the behaviour of internal discharge in a solid or liquid insulation under AC voltage. A capacitance C_c indicates the capacity in the cavity where the discharge is produced, the capacity of the insulation in series with the cavity is defined by a capacitance C_b and the sound part of the insulation is defined by a capacitance C_a[23].
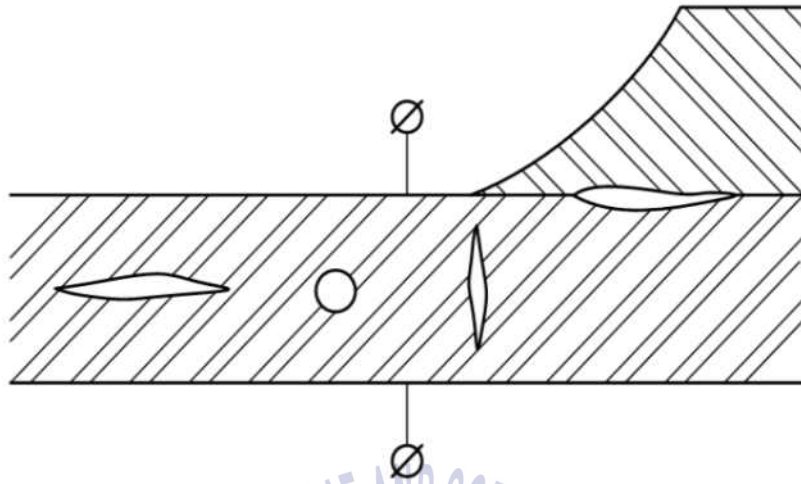
Fig. 2.4 Internal discharges
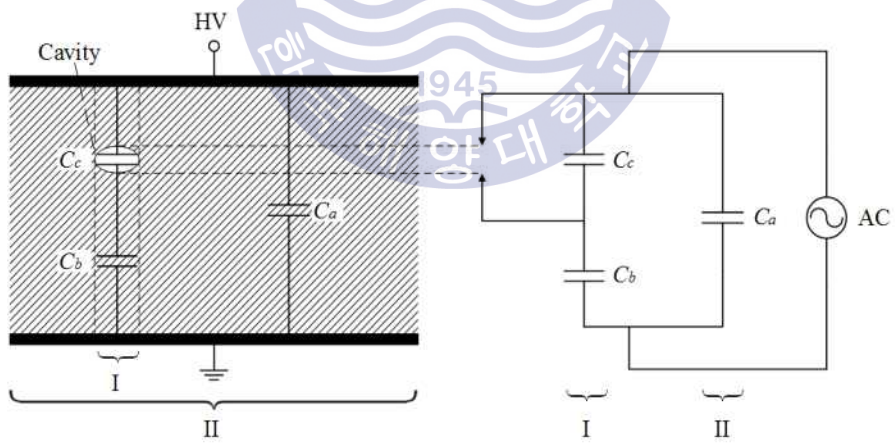
Fig. 2.5 Equivalent circuit of internal discharge under AC

The total capacitance of the equivalent circuit is equal to:

$$C = C_a + \frac{C_b C_c}{C_b + C_c} \tag{2.4}$$

If AC voltage $V_a = V_m \sin\omega t$ is applied to this sample, the voltage across the cavity V_c is equal to:

$$V_c = \frac{C_b}{C_b + C_c} V_m \sin\omega t \tag{2.5}$$

which is represented in dotted line as shown in Fig. 2.6. When the voltage V_c reaches voltage U^+, a discharge occurs in the void. On the other hand, when the voltage drops to V^+, the discharge extinguishes. The voltage U^+ is called partial discharge inception voltage (DIV) and the voltage V^+ is called partial discharge extinction voltage (DEV), respectively.
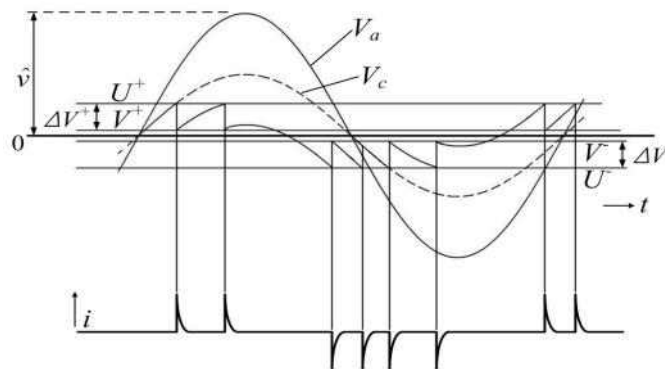
Fig. 2.6 Recurrence of discharge

A discharge extinguishes in the cavity and generates a current impulse. This process proceeds in less than 10^{-7} s, so the current impulse appears a vertical line of corresponding phase. As the applied voltage is increased, the discharge reoccurs when V_c reaches U^+ again. The same phenomenon is represented at the negative half of the applied voltage.

Transfer charge q_t released from the cavity is equal to:

$$q_t = (C_c + \frac{C_a C_b}{C_a + C_b})(U - V) = (C_c + \frac{C_a C_b}{C_a + C_b})\Delta V \qquad (2.6)$$

while $C_a \gg C_b$, thus

$$q_t = (C_b + C_c)\Delta V \qquad (2.7)$$

However, q_t cannot be detected and therefore it is not a practice to evaluate PD. The voltage drop ΔV caused by a discharge distributes inversely with capacitance C_a and C_b, the voltage drop in capacitance C_a is equal to:

$$\Delta V_a = \frac{C_b}{C_a + C_b}\Delta V \qquad (2.8)$$

which means there will be a voltage drop in the sample when discharge occurs in the cavity. The corresponding charge q released from the test object is equal to:

$$q = (C_a + C_b)\Delta V_a = C_b \Delta V \qquad (2.9)$$

The discharge magnitude q is represented as apparent charge, which is the most important parameter for evaluating PD and normally expressed in picocoulomb (pC). In IEC 60270, if the apparent charge q is injected within a very short time between the terminals of the test object, it would give the same reading on the measurement instrument as the PD current pulse itself. The measurement of apparent charge must be carried out by calibration process to determine the scale factor k. By comparing equation 2.7 with 2.9, the ratio of q to q_t is given by:

$$\frac{q}{q_t} = \frac{C_b}{C_b + C_c} \qquad (2.10)$$

When the proportional relation between apparent discharge and transfer discharge is verified and q can be used to measure PD[23],[24].

2.2 Typical PD sources in GIS

Dielectric breakdown is caused by insulation defects in GIS during the commissioning or in service. The PD activity is produced by many of these insulation defects before insulation breakdown finally occurs. Therefore, it is very important to detect these PD signals before GIS fails. Fig. 2.7 shows typical PD sources in GIS[11],[25]-[27].
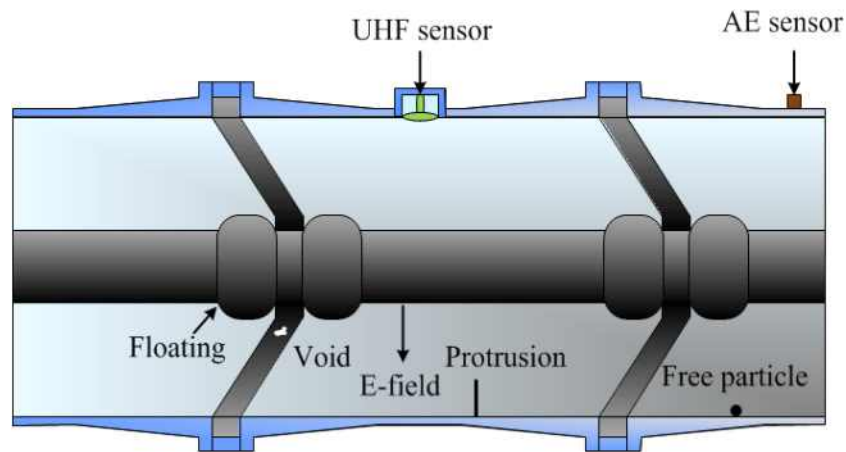
Fig. 2.7 Typical PD sources in GIS

a) Free moving particles

Despite all the precaution taken during the processes of production, assembling, transportation, and switching operation of the GIS, metallic particles may exist inside GIS compartments. The shape, location, and orientation of the particle determine the induced charge distribution. When the high electric field is concentrated surround the particle, it can move under the influence of the electric field. Depending on the strength of electric field and the accumulated charge on the particle, it is known that the particle can have one of the following moving stages; shuffling, moving, and jumping. The first movement stage is the shuffling particle. In this stage, the particle is not yet moving, but gives contact-noise-like discharges. In second movement stage, the local electric field exceeds the gravitational force and the particle begins moving up and down. If the gravitational forces are greater than electrical forces in the low field region and it reaches a high

- 18 -

stress region, finally the particle starts to jump and may reaches HV conductor, which leads to breakdown. The PD signals of the free moving particle are relatively easy to be detected by both conventional and non-conventional methods[27]-[31]. Fig. 2.8 shows an example of the free particle.

Fig. 2.8 A curly-shaped aluminium particle

b) Floating elements

Incorrectly fixed or unscrewed elements cause vibration of the GIS and they can loose their contact with the conductor. When the withstand voltage between the HV electrode and the floating element exceeds the insulation strength of the gas, an electrical discharge occurs. Such discharge tends to be repetitive with a charge transfer in the range from thousands to millions of pC. The floating PD signals are also easily detected by any kind of electrical PD measurement like free moving particle as mentioned above. It produces a

much higher magnitude than other defects and PD pattern is usually regular and presents high amplitude and high pulse count[11],[29],[31]. Fig. 2.9 shows an example of the floating element.

Fig. 2.9 A loose bolt and nut inside GIS

c) Voids

The spacer is used for holding the conductors and for dividing the compartment of GIS chambers. Voids are result from air bubbles produced during the manufacturing process of solid spacers, such as high temperature casting and curing of epoxy. Voids in spacers or delamination of a solid insulator from electrodes are usually filled with a low-pressure gas mixture. When the electric field within the void exceeds the discharge inception field, the first free electron is available. Once the electric field is sufficiently high, PD occurs by electron avalanches as mentioned in Chapter 2.1. When a PD in epoxy spacer proceeds for a long time of period, it can also lead to

treeing, eventually insulation breakdown. To detect such defects, electrical PD measurements in the factory are used but void discharges are required to apply the voltage for a period of time to become active depending on void size. Furthermore, such voids are very difficult to be detected in the factory testing if the void size is smaller than 1 mm, generating very low amplitude less than 10 pC. It was also shown in experiments that the statistical time delay was in the order of 30 minutes for 1 mm-void and around 3 days for 200 μm-void. Thus, it may be difficult to detect the small void for 60 seconds based on IEC 62271-203[27],[32]-[36]. Fig. 2.10 shows an example of the void.

Fig. 2.10 A void detected by X-ray in an insulator

d) Protrusions

When the electric field is concentrated on the protrusion tip, a corona discharge occurs under local electrical field stress. Typically these defects are divided into rounded protrusion and sharp protrusion. The rounded protrusion

is very difficult to be detected due to the small difference between the PD inception voltage and the breakdown voltage. In case of the rounded protrusion on conductor, the breakdown occurs rapidly despite small increase in the test voltage. The sharp protrusion is relatively detected easily by electrical PD measurement due to sufficient difference between the PD inception voltage and the breakdown voltage. PD inception voltage depends on the length of the protrusion. Corona discharge by sharp protrusion does not cause immediate breakdown because the corona stabilization reduces locally the electrical field[11],[29],[37],[38]. Fig. 2.11 shows an example of the protrusion.

Fig. 2.11 A protrusion on enclosure

Depending on types of defects, the critical and detectable lengths are specified in the CIGRE technical brochure 525. Table 2.1 shows the critical and detectable length for different defects. The detectable values were obtained by conventional PD measurement according to IEC 60270. Each

- 22 -

defect generates the PD signal but its magnitude of pC may be very low depending on the length and location of the defect, as well as the nominal voltage of the GIS[11].

Table 2.1 Critical and detectable length for different defects

Type of defect	Critical defect		Detectable length of defect at U_n
	Length	Apparent charge According to IEC 60270	
Moving particle	3−5 mm	2−10 pC	3-5 mm
Protrusion on HV conductor	around 1 mm	1−2 pC	3−4 mm
Protrusion on enclosure	1-2 mm	about 0.5 pC	3−10 mm depending on location
Void	3−4 mm (diameter)	1−2 pC	2-3 mm depending on location

2.3 Technical methods and strategies for PD diagnosis

The techniques for PD diagnosis have been developed to improve their sensitivity for over 40 years and they are used for laboratory and on-site applications worldwide. Based on physical phenomena accompanied with PD, PD diagnosis for GIS can be categorized into a conventional method based on IEC 60270 and non-conventional methods including UHF and AE methods. The conventional method is used when test objects are energized to detect PD signals by external voltage sources. It has high sensitivity due to

precise measurement and it can measure and display PD magnitude in pC. However, a coupling capacitor is necessary for quantitative measurements and it cannot be installed during operation of power facilities. Since the conventional method is likely to affected by on-site noise interference, it is usually used for laboratory and factory testing. Meanwhile, many of non-conventional methods have been studied for the on-line application, and UHF and AE methods of them are widely used to monitor GIS condition continuously due to their advantages. However, it is impossible for them to measure direct PD magnitude and they are affected by the attenuation of PD signals with increasing distance from PD origin. Therefore, it is very important to understand their advantages and disadvantages and perform strategic PD diagnosis depending on the laboratory and on-site condition monitoring for PD measurement. Fig. 2.12 shows technical methods for PD diagnosis applied for GIS under on-site monitoring[39].
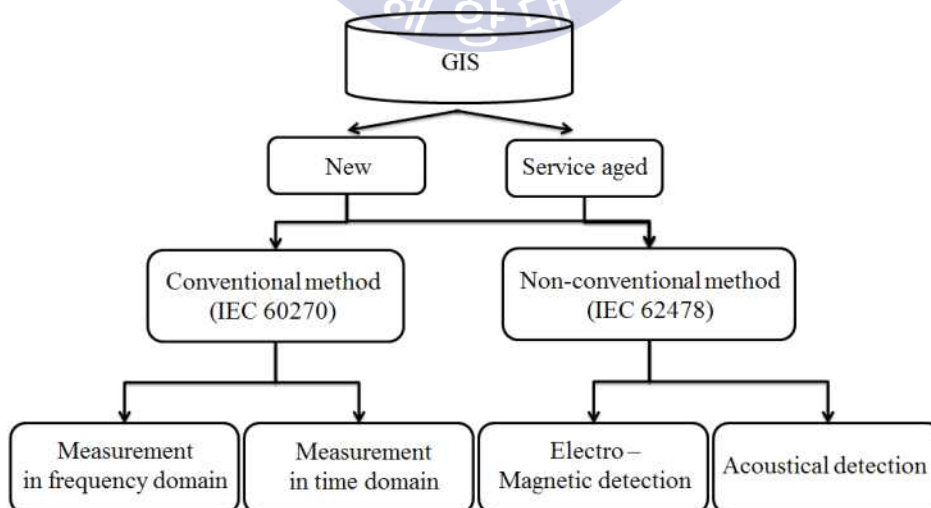
Fig. 2.12 Technical method for PD diagnosis under on-site monitoring

a) Conventional method

PD diagnosis of new GIS during factory testing is typically performed with the standard conventional test circuit based on IEC 60270. Fig. 2.13 shows basic diagram of a PD detection. The test circuit consists of input impedance of measuring system Z_{mi}, test object C_a, coupling capacitor C_k, and other measuring instruments (MI). When a PD occurs in the test circuit, discharge current flows through the coupling capacitor and the voltage signal is detected by the measuring impedance. The amplitude of voltage signal can be calibrated in pC by coupling device and measuring instruments[10],[19].

Fig. 2.13 Basic diagram of a PD detection

Before the PD is measured, it should not be generated excluding the test object, and the calibration procedure in compliance with IEC 60270 should be carried out by injecting current pulses with known charge magnitude into the terminal of the test object. The advantage of conventional method can be reproducible and comparable PD test results by the calibration procedure,

- 25 -

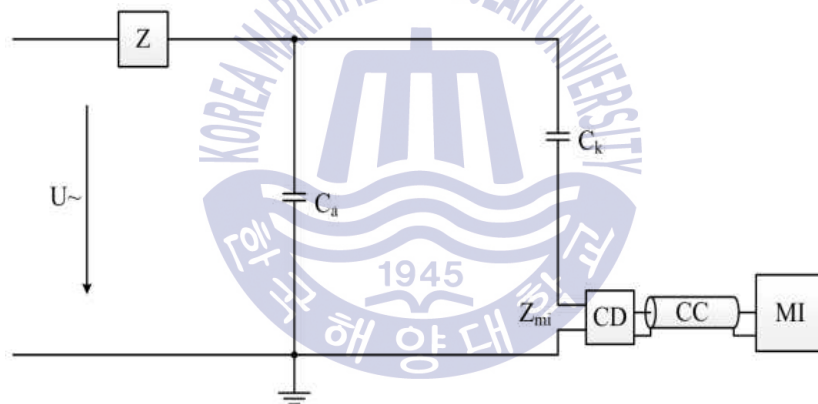even though the test is performed by different PD measuring devices with other on-site engineers. Thus, the pass or fail criteria can be established by comparing the PD level of the GIS under test with set limits. For this reason, the conventional method has been accepted as the standard method for PD testing worldwide[11],[27],[29],[39],[40].

When on-site PD measurement is performed according to the conventional method in compliance with IEC 60270, the signal-to-noise (S/N) ratio is poor since its maximum measuring frequency is below 1 MHz. The sensitivity of the conventional method is strongly reduced by the poor S/N ratio by external interference because the background noise level may range from a few tens to a few hundreds of pC depending on surrounding environment. It is also difficult to locate PD sources with the measuring frequency of 1 MHz which translates to a wavelength of 300 m, making PD localization impossible. As a result, acoustic methods are often employed during factory testing. For this reason, the conventional method has been substituted by non-conventional methods such as UHF and AE methods[10],[27],[39],[41],[42]. Table 2.2 shows strengths and weaknesses of the conventional method[43].

b) UHF method

UHF method for PD diagnosis started to appear in the early 1980s and is widely applied to detect and locate PD signals in a GIS under on-site measurement. It is quite successful for continuous monitoring of the GIS condition and more recently the application of the UHF method was extended to high-voltage power transformers for condition monitoring. When a PD occurs, electromagnetic waves in frequency ranges from 300 MHz to 3 GHz

Table 2.2 Strengths and weaknesses of a conventional method

Strengths	Weaknesses
• can be calibrated in pC according to IEC 60270 • restricted bandwidth • a complete GIS section can be surveyed by one system	• very difficult to apply at in service HV GIS and at voltage levels above 300 kV • a coupling capacitor is necessary for quantitative measurements • invasive (in terms of gas compartments when an encapsulated coupling capacitor is used) • susceptible to noise interference on-site • no options for PD defect localization

produced by the PD source propagate inside the GIS enclosure, the signals are detected by UHF sensors installed on the GIS windows or spacers. There are many advantages of UHF method and one of them is excellent S/N ratio. The frequency spectrum of the electromagnetic wave ranges up to 3 GHz because PD pulses in GIS have very short rise time below 1 ns, especially from defects of insulating materials such as voids and cracks. Most of electromagnetic noise in the GIS occur at low frequency range below several MHz. Therefore, it is likely to suppress noise by detecting the PD signal at higher frequency ranges from a few hundred of MHz to GHz. Then, the S/N ratio for UHF method will be improved. The reason why noise tends to

predominate at the lower frequency is that electromagnetic waves are typically attenuated more strongly at high frequencies when propagating in the GIS enclosure. Since noise is produced further from a PD sensor than the PD source, it is more attenuated at higher frequencies than the PD source. Also, the UHF method has the good performance to identify different types of PDs using different frequency and time domain characteristics[39],[44]-[47].

Although there are many strengths of UHF method, the main disadvantage is that it is impossible to measure PD magnitude in pC because the remote UHF sensor detects electromagnetic signals propagated from a PD source with an attenuation. Therefore, The PD signals measured by the UHF method depend on the following factors; location of the defect within the GIS compartment; propagation effects including reflection, interference, and attenuation; the position of sensor relative to the defect and the signal propagation path; types of UHF sensor. It is meant that it cannot be calibrated in terms of pC, resulting in different PD test results depending on the factors as mentioned above. To overcome the disadvantage, many studies for comparison of UHF measurements with the standardized PD measurements defined by IEC 60270 have been actively carried out and there are correlation between UHF and conventional measurements in Fig. 2.14[41]. Alternatively, sensitivity check of UHF sensors can be performed using a pulse generator during on-site measurement and has proven to be useful for GIS by CIGRE Task Force 15/33.03.05[25],[27],[48]-[51]. Table 2.3 shows strengths and weaknesses of the UHF method[43].
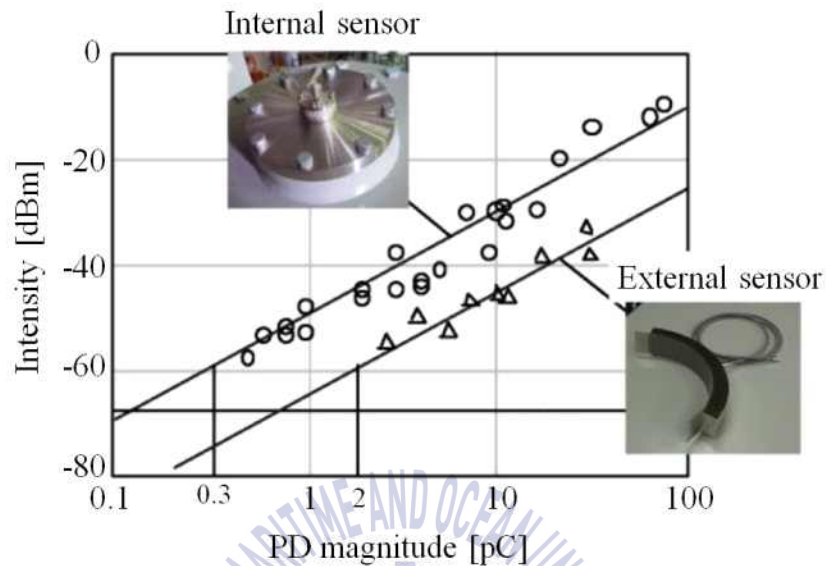
Fig. 2.14 A pC-dBm correlation by UHF sensors

Table 2.3 Strengths and weaknesses of an UHF method

Strengths	Weaknesses
· high sensitivity when using internal PD sensors · possibility to be retrofitted (occasionally with lower sensitivity) · allows continuous PD monitoring · localization of PD defects possible · same life expectancy of all types of UHF sensors compared to GIS	· sensitive external noise signals (increased level of interference) · cannot be calibrated in terms of pC (minimum detection sensitivity can be ensured) · long-term behaviour of electronic components · not always applicable to all types of GIS

c) AE method

AE signal emitted by PD events causes mechanical vibration and is detected simply by AE sensors mounted on the outside of GIS enclosure. Most of fundamental researches for AE techniques has been performed since the 1990s and the AE method is widely accepted and suitable for PD diagnosis of GIS during commissioning and in-service testing until now. When a PD occurs, acoustic signals are transmitted from the PD source, the piezoelectric element of the sensor can respond to this signals and transduce them into electrical signals. It is sensitive enough to detect PD sources such as moving particles, floating elements, and protrusions using measuring frequency ranges from 10 kHz to 300 kHz. The AE method has many advantages of easy retrofit and high immunity to electromagnetic noise, and especially the main advantage of AE method is to locate the PD source using time of flight (TOF) technique and it has been proven for PD location in many cases of on-site measurement[42],[47],[52],[53]

Although the AE method is suitable for PD diagnosis of on-site measurement, it cannot be obtained in terms of pC, as mentioned like UHF method. Its sensitivity is also highly dependent on the PD defect and its location because the acoustic wave propagated from the PD source to the AE sensor is strongly influenced by the signal propagation path and SF_6 gas pressure. So it is very difficult to detect defects of insulating materials such as voids and weak surface discharges due to high attenuation. In any cases of on-site measurement, the preamplifier is usually required to detect PD signals because vibrations produced by the PD source are relatively weak. Thus, the acoustic method is commonly not applicable for comprehensive

- 30 -

continuous monitoring for PD diagnosis in a substation due to the necessity for installation of many acoustic sensors[27],[29],[41],[53],[54]. Table 2.4 shows strengths and weaknesses of the AE method[43].

Table 2.4 Strengths and weaknesses of an AE method

Strengths	Weaknesses
• able to be applied on in-service • occasionally less sensitive to noise interference • simple to use for localization of a PD defect • comparatively cheap and easy to carry equipment • good applicability in case of access to gas compartments • non-intrusive	• sensitivity is highly dependent on the PD defect and its location • time consuming in case of complete GIS survey • occasionally high amount of manual work • sensitive to rain in case of outdoor GIS, to mechanical impact, and to magnetostriction (resulting from inductive voltage transformers) • not applicable for continuous PD diagnosis as per common practice • cannot be calibrated in terms of pC

Before using technical methods as mentioned above, it is very important to establish the strategies of PD diagnosis. The users such as utilities, companies, and laboratories have to decide periodic, temporary continuous or

continuous measurement considering types, specifications and criticality of target subjects. CIGRE WG B3.24 defines three different time-based strategies, which can apply to on-site PD diagnosis as shown in Table 2.5[43].

Table 2.5 Overview of different time-based strategies of PD diagnosis

Strategies	Periodic	Temporary continuous	Continuous
Description	· Limits of connected location for a limited time	· A few connected locations for a limited time	· All locations without time limitation
Advantage	· Flexible use	· Flexible use · Tracking of every discharge occurring in time window · Time history trend analysis · Alarm generation · Remote control	· Tracking of every discharge · Time history · Trend analysis · Alarm generation · Remote control
Drawbacks	· No PD diagnosis between two campaigns · non- detection of intermittent PDs	· Specific algorithms are required to eliminate noise interference · Expert system software is required	· Specific algorithm are required to eliminate noise interference · Expert system software is required
Time scale	· 1 ⋯ 2 day	· 1 week ⋯ 1 year	· GIS life time
Relative cost	· Lowest initial costs	· In the mid-level	· Highest intial costs

2.4 PD analysis methods

Many studies of the PD analysis techniques have been performed to find defects in GIS and remove them during maintenance because it takes a long time to find them without any information of defect types and locations. The PD analysis techniques are mostly performed in the frequency and time domain. The frequency and time domain measurements are usually used to identify insulation defects and to classify their types, respectively. In this chapter, the strengths and weaknesses of each method are described.

a) Phase-resolved partial discharge (PRPD) in time domain

The PRPD analysis is commonly adopted and widely used to classify types of PDs by electrical measurements worldwide. Every PD activity is always a sequence of PD pulses with their magnitude (q) and time (t) of discharge occurrence, which is called phased resolved PD sequence (PRPS) record. The PRPD patterns are characterized using PD data including phase angle (Φ), magnitude (q), and number (n) of discharge occurrence by overlapping PD pulses within one cycle of the applied voltage, as shown in Fig. 2.15. The PD identification can be analyzed using the PRPD patterns accumulated within a certain time. These PRPD patterns are also strongly influenced by the level of AC test voltage applied to GIS. Therefore, precise diagnosis of insulation defects can be performed successfully only if several PD parameters are evaluated simultaneously[11],[39],[55],[56].

In the PRPD method, PD pulses have to be accumulated within a certain time. However, it is difficult to identify the PD pulses from external noise and interference and to determine whether it is a PD source or not when high
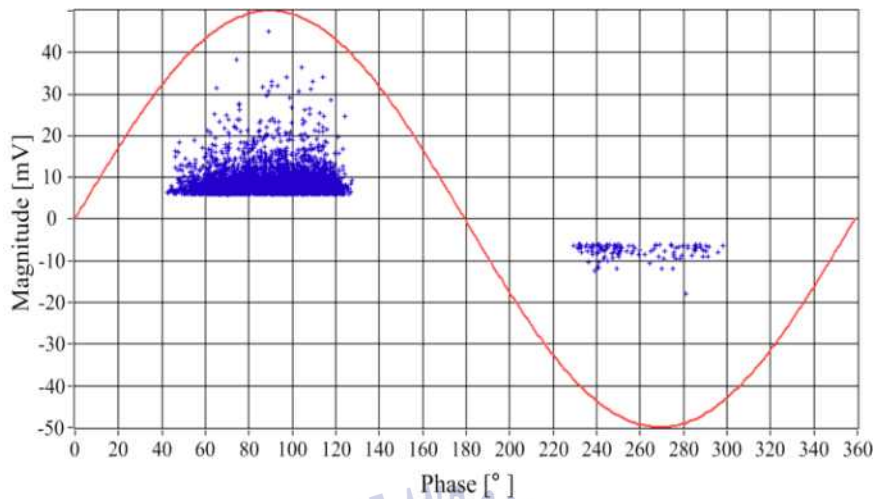
Fig. 2.15 An example of PRPD pattern

levels of external noise and interference are continuously present. The external noise and interference can be removed by the noise gating technique but there are disadvantages that the noise sensor must be required further and original PD signals occurring in same time with the noise signals must be removed. Further, if there is no algorithm to determine types of PDs, high level of expert's knowledge and experience are required for precise PD diagnosis.

b) Frequency and phase spectrums

The frequency spectrum analysis is mainly performed to identify PD signals in comparison with noise signals. The frequency components depend on the rise time of the signals so the short rise time of PD signals below 1 ns have higher frequency spectrums than noise signals. In addition, it is known that PDs have specific frequency spectrum in many cases of on-site

measurement as well as that the noise is suppressed as the frequency spectrum increases. Therefore, The frequency spectrum analysis method is very useful to distinguish between PD and noise signals, as shown in Fig 2.16[57]. It is, however, difficult to classify types of PDs by using only frequency spectrum analysis.
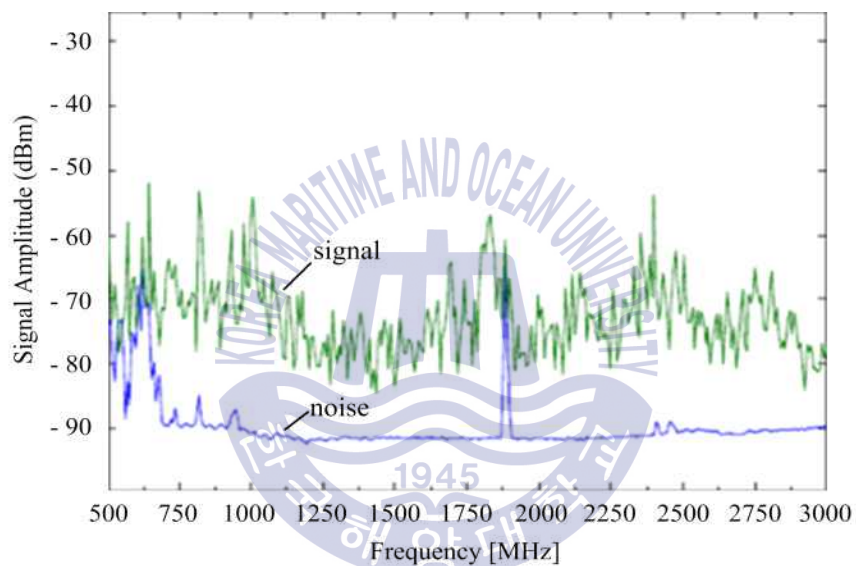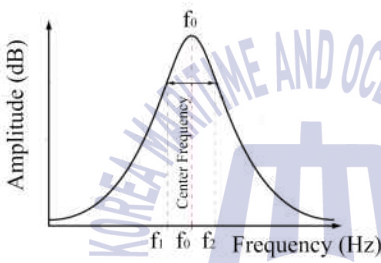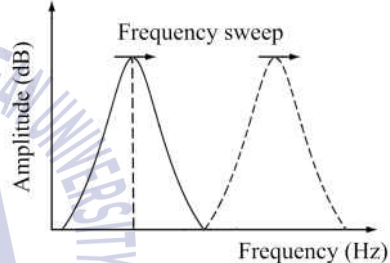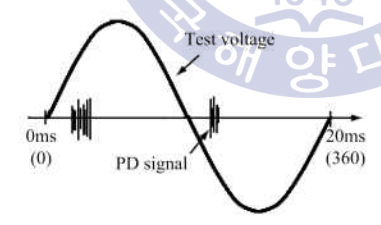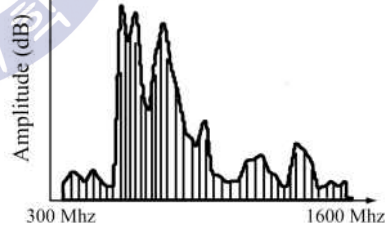

Fig. 2.16 Frequency spectrum analysis

The UHF method for PD diagnosis is mostly performed in the frequency domain using either the zero span or the full-spectra modes as described in Table. 2.6. When PD pulses are analyzed by frequency spectrum using zero-span mode, time-domain PD signals are obtained at the maximum peak frequency by setting spectrum analyzer. The time-domain PD signals for optimal sweep time are transferred to the phase spectrum including phase

angle (Φ) and magnitude (q) of discharge occurrence. Fig 2.17 and Fig 2.18 shows examples of configuration for the combined method and examples of frequency and phase spectrums measured by the combine method, respectively[11],[27],[39],[58].

Table 2.6 Frequency-domain measurement

Principle	Zero-span mode	Full-spectra mode
Frequency analysis		
PD analysis		

Fig. 2.17 A configuration of a combined method

(a) Frequency spectrum

(b) Phase spectrum

Fig. 2.18 Frequency and phase spectrums of a protrusion
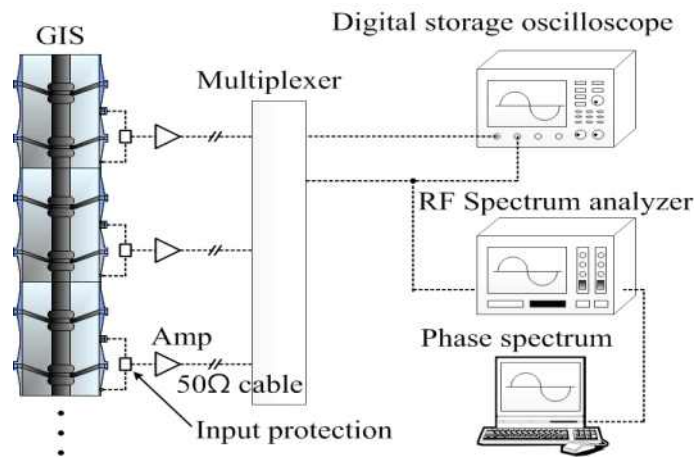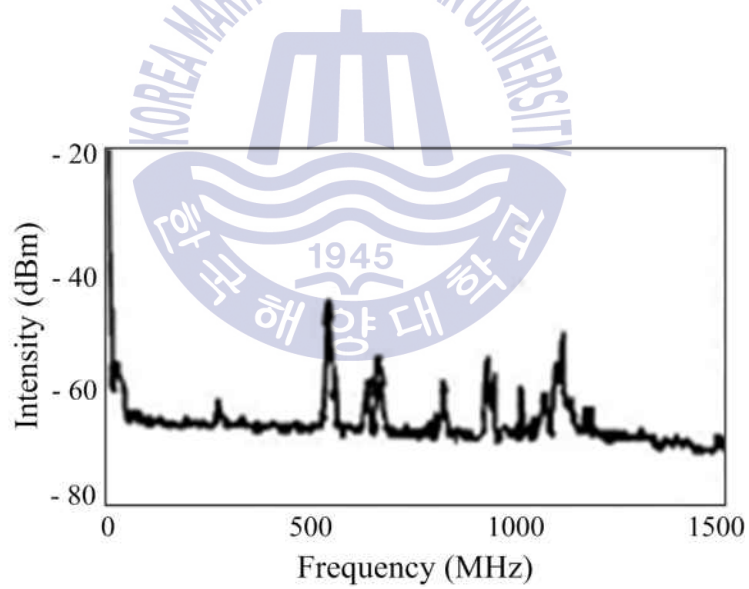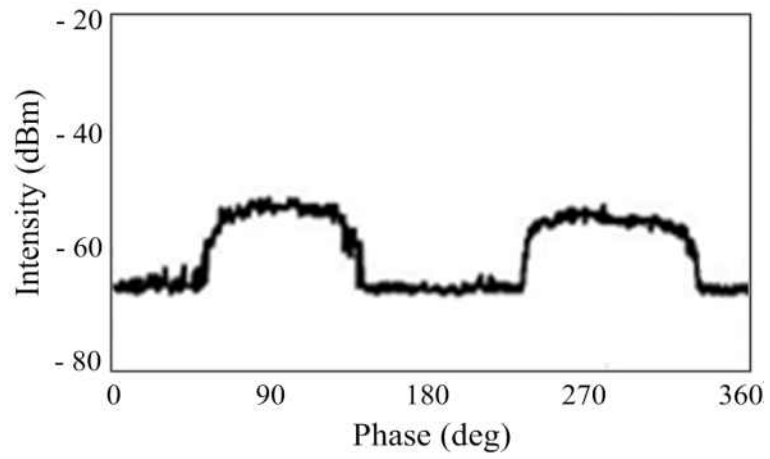
Chapter 3 Data Acquisition and Analysis

As mentioned in Chapter 2.4, the parameters of PD analysis methods are very useful to classify and identify types of PDs. The discharge phase is one of the most important parameters, especially with respect to PD classification in both PRPD and combined methods. The diagnosis results by the portable UHF PD device were not correct in many cases of on-site PD measurement, as investigated by comparing with the inspection results. This was because most of the UHF PD measurements were conducted without phase synchronization with the applied voltage. To acquire the phase angle of the voltage applied to GIS, the voltage terminal in the PT of GIS is connected to the UHF PD system. This is not an easy task to complete in the field because most customers have a reluctance to use the PT signal due to its perceived tendency to malfunction during service. For example, in Korea, when use of the PD signal is not approved for the UHF PD device, the voltage of AC 110/220V is commonly used to identify PD occurrence but the phase differences occurs between the voltage of a few hundred kV applied to GIS and the voltage of AC 110/220V used in the substation as shown in Fig. 3.1. It is also impossible to classify PD types in three-phase construction because it is difficult to obtain the phase in which PD occurs of three phases[59],[60]. The phase-asynchronous PD patterns would give an incorrect diagnosis and it is difficult to take the proper actions for maintenance. Therefore, a new method of PD diagnosis was designed to identify types of 6 PDs and 4 noises clearly. Fig 3.2 shows the block diagram of a development process for the new PD diagnosis method.
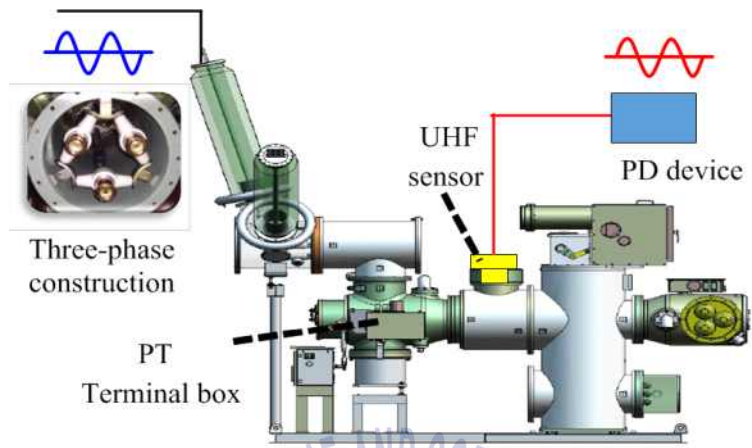
(a) On-site PD measurement
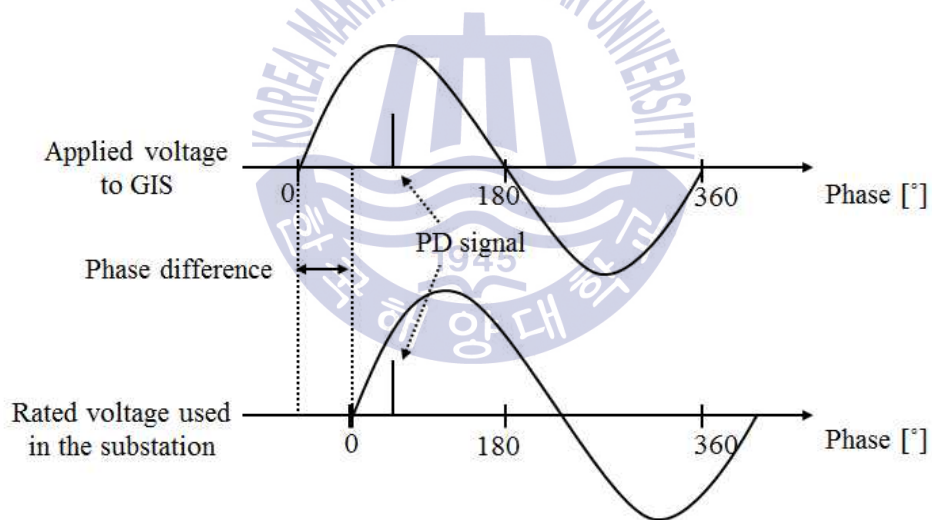
(b) Phase differences

Fig. 3.1 Phase differences of on-site PD measurement

```
┌─────────────────────────┐
│   Data acquisition      │
│   -327 data             │
└─────────────────────────┘
            │
            ▼
┌─────────────────────────────┐
│ Reviewing data validation   │
│ - Selecting the reference   │
│   data                      │
└─────────────────────────────┘
            │
            ▼
┌─────────────────────────────┐
│ Feature extraction          │
│ - Frequency : 5EA           │
│ - Phase : 6EA               │
└─────────────────────────────┘
            │
            ▼
┌─────────────────────────────┐
│ Selecting valid parameters  │
│ - Frequency : 3EA           │
│ - Phase : 2EA               │
└─────────────────────────────┘
            │
            ▼
┌─────────────────────────────┐
│ New PD diagnostic model     │
└─────────────────────────────┘
```
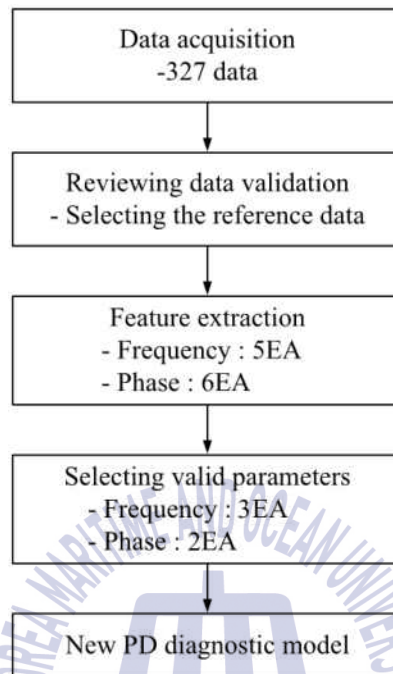
Fig. 3.2 Block diagram of a development process

3.1 Statistical analysis

The 327 cases of PD measuring data were collected from 2003 to 2015, including 297 cases of on-site PD measuring results in 26 domestic and overseas substations, 23 cases of PD results during factory test, and 7 cases of typical UHF PD data. The PD measurements were performed by on-site engineers for GIS subjects of 24 kV to 800 kV.

To construct PD database, the data sample consists of measuring information, PD measuring result, shapes, characteristics of frequency and phase spectrum, internal inspection, PD location, and on-site engineer's interview, as shown in Fig. 3.3.

GIS PD Case (No.1)					
■ File Name : PD Diagnosis Data (2003-2008)					
Measuring Information					
Measuring Date	Substation	Measuring position	Target GIS	Sensor Type	Amp
2003.08.05	S/S	No.1 Main BUS	170kV	External	25dB
Measuring Results					
PD Situation		Maximum Frequency (MHz)	Maximum Signal (dBm)	iPDM Diagnosis	Internal Inspection
PD generated in all ranges in No.1 Main Bus		1301	-31.08	Protrusion	Crack
Frequency Pattern			**Phase Pattern**		

Frequency Characteristics	**Phase Characteristics**
1. Frequency Ranges : From 1G to 1.5GHz 2. Frequency Density : High from 1G to 1.5GHz 3. Frequency Magnitude : Mainly generated under -30dBm	1. Phase Ranges : One area from 230˚ to 300˚ 2. Phase Magnitude : -30dBm 3. Phase Shape : Pentagon / Square
Internal Inspection	**PD Location**
Post Insulator Crack	

Engineer Interview

1. Fault Cause : <u>Crack</u>
 2. Fault Location : <u>Post Insulator of Main Bus</u>
 3. Interview Results
   - PD occurred continuously for a year
   - The GIS operation halted and replaced at site
   - After inspection, PD stopped
 4. Risk Level : Condition 3

Fig. 3.3 An example of PD data

Faulty GISs were visually inspected by experienced engineers and maintenance experts. Most of on-site PD measurements were conducted without phase synchronization using the UHF PD device (Model : HiCMS

GM−100) developed by Hyosung corporation. As mentioned above, although the UHF PD device was equipped with diagnosis algorithm for classifying types of PDs, the diagnosis results were not correct in many cases of PD data because the phase spectrums resulting from the phase-asynchronous PD signals were different from those of actual PD types. After data acquisition, the database of 225 cases were constructed by arranging 327 cases of PD measuring data. The statistical analysis was performed according to types of defects, types of PDs and noises, compartments and components, and voltage classes and actions taken for inspections as follows.

a) Types of Defects

The first largest portion of inspection results was PDs about 63 % as illustrated in Fig. 3.4. In case of the unknown causes, abnormal signals like the PD signal were detected during on-site PD measurement but the defects were not founded by the on-site engineer and their causes were not clear. Therefore, they were excluded from the database.
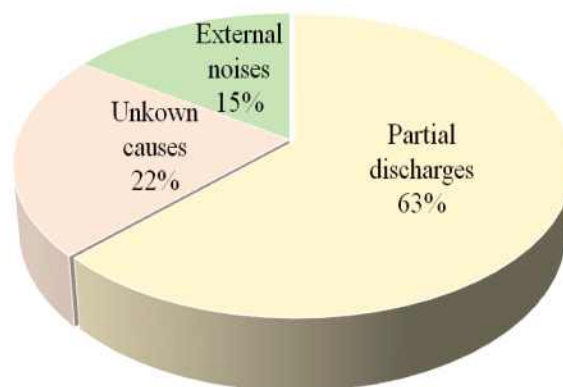

Fig. 3.4 Distribution of defect types

b) Types of PDs and noises

In Fig. 3.5, the most frequent PD cause was the floating element about 70 %. In case of the transformer (TR) faults about 6 %, when a PD signal was detected by the UHF PD sensor installed on GIS and precise PD diagnosis was performed by on-site engineers, it was shown that the PD signal was caused by the high-voltage transformer, which was connected near the GIS. The electromagnetic signal may be propagated from the transformer to the GIS. The protrusion and free particle rarely occurred.
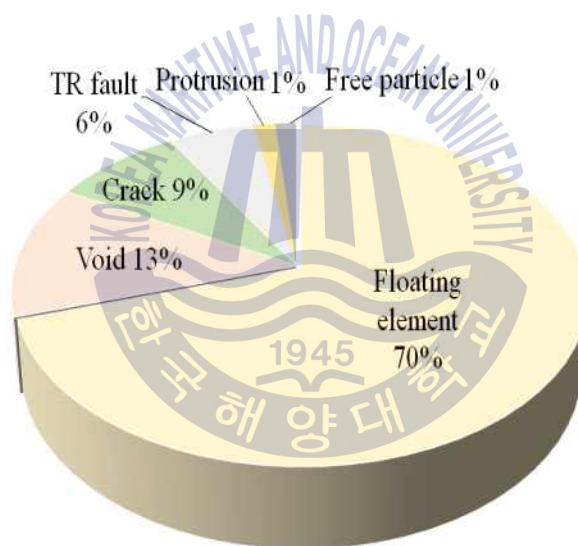

Fig. 3.5 Distribution of PD types

The most frequent noise was the external interferences about 40 % as shown in Fig. 3.6. In case of the sensor connector faults, the abnormal signal was detected like the PD signal and the signal level was much higher than others like the floating element when the contact failure between UHF sensor connectors occurred in some cases.
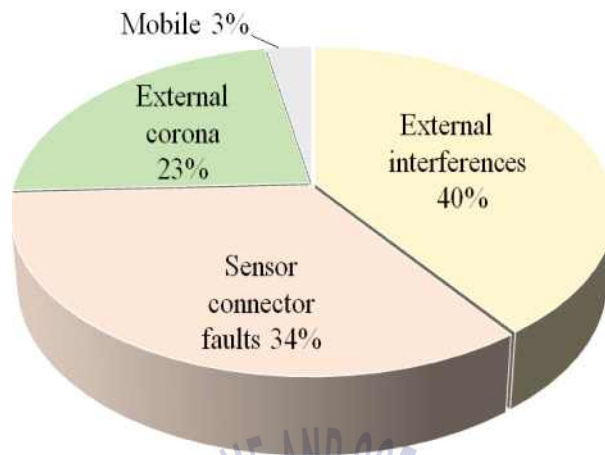
Fig. 3.6 Distribution of noise types

c) Compartments and components

The most frequent GIS compartments in which PD occurred were the gas-insulated breaker (GIB) and disconnect switches(DS) about 34 % and 31 %, respectively as illustrated in Fig. 3.7. In case of the most frequent GIS components in which PD occurred, the bolts and washers were 41 % and 26 %, respectively. PDs from the conductors, tulips, and contacts were rarely generated. Fig. 3.8 shows relative distribution of GIS components where PD occurred. The faults in cases of GIS compartments and components were excluded.

Fig. 3.7 Distribution of GIS compartments

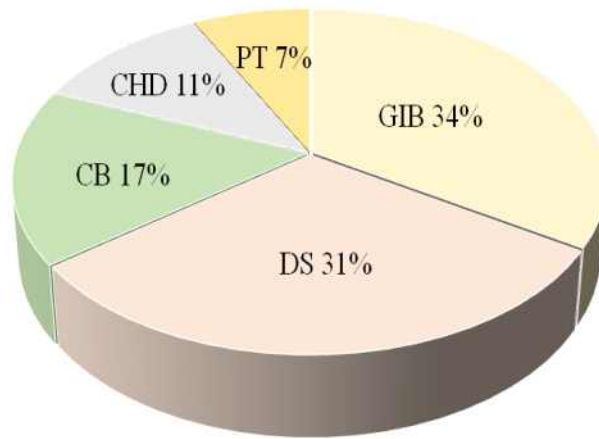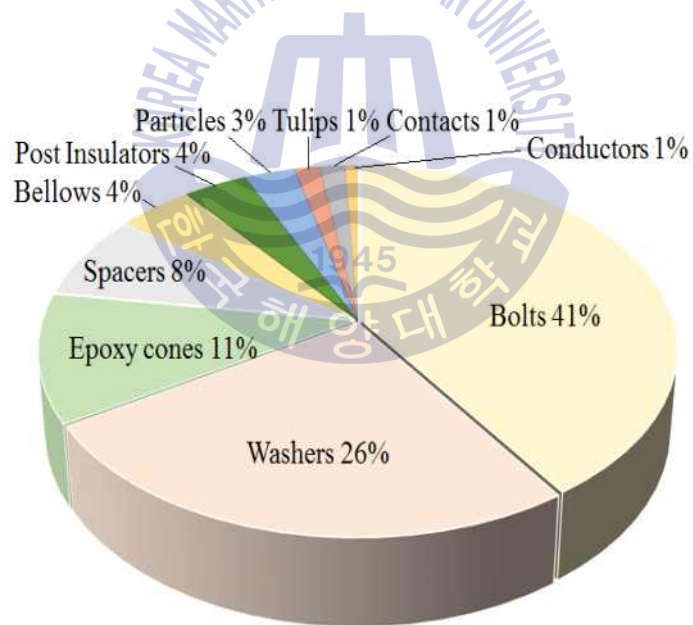Fig. 3.8 Distribution of GIS components

d) Voltage classes and actions taken for inspections

In the database as shown in Fig. 3.9, the highest relative portion of

voltage classes at which PD occurred were 362 kV and 170 kV about 64 % and 26 %, respectively. The remaining voltage classes had low relative portion of total 10 %. In case of actions taken for inspections, the most frequent actions were internal inspections and replacements about total of 76 % when PDs occurred. The external inspections of 24 % were followed. Fig. 3.10 shows the relative distribution of actions taken for inspections.

From the statistical analysis, the first largest portion was PDs about 63 %, resulting from on-site PD measurement and the most frequent PD types were the floating elements of 70 % and then followed by 22 % of the defects of insulating materials such as voids and cracks. In case of external noises, the most frequent causes were external interferences and sensor connector faults over 70 %. When a PD was detected, the most frequent GIS compartments and components in which PD occurred were GIB about 35 % and bolts about 41 %, respectively. Also the largest portion of voltage classes was 362 kV and the internal inspections and replacements were performed over 70 % once the PD signals were detected. Defect types and PD correlation between compartments and components were classified, respectively in Table 3.1 and Table 3.2.
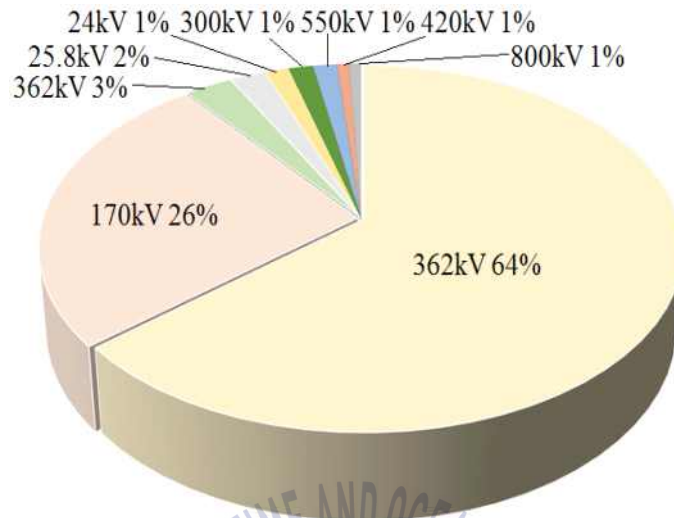
Fig. 3.9 Distribution of GIS voltage classes
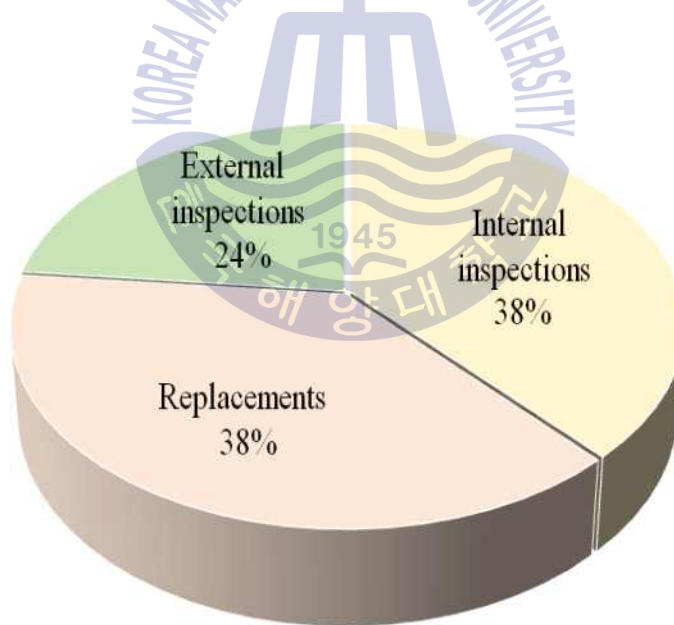
Fig. 3.10 Distribution of actions taken for inspections

Table 3.1 Classification of PD and noise types

Classification	Types of causes
PDs	Floating element
	Free particle
	Protrusion
	Crack
	Void
	Transformer(TR) fault
Noises	External interference
	Sensor connector fault
	External corona
	Mobile

Table 3.2 PD correlation between compartments and components

PD types	Compartments	Components
Protrusion	GIB	Particle
Void	CHD	Epoxy cone
	GIB	Spacer
		Insulator
Free particle	GIB	Particle
Crack	GIB	Spacer
		Insulator
Floating	CB	Bellow
		Bolt
	DS	Washer
		Tulip contact
		Bolt
	GIB	Conductor
		Bolt
		Tulip contact
	PT	Bolt
TR fault	TR	TR

3.2 Feature extraction

To develop the new method of PD diagnosis which is applicable to the on-site PD diagnosis without phase synchronization, the features were extracted to classify defect types using the representative data of 82 cases including 66 PDs and 16 noises. The representative data were selected through a review of data validation to eliminate the duplicated data in the same GISs and the uncertain data for the result of internal inspection by on-site engineers and PD diagnosis experts.

The features of various frequency and phase parameters were extracted because the frequency and phase spectrums of PD signal were analyzed by the UHF PD device in all cases of the database. They consisted of 5 frequency parameters and 6 phase parameters. The 5 frequency parameters were the number of distribution ranges, maximum value, frequency ranges of first and second peak values, peak differences between first and second values, and density levels. 6 phase parameters were defined as: the number of phase groups, overall distribution ranges or not, distribution ranges of each group, density levels, peak differences between the first and second groups, and shapes The frequency and phase parameters are detailed in 3.2.1 and 3.2.2 chapters.

### 3.2.1 Criterions of frequency parameters

a) The number of distribution ranges

Frequency ranges were divided into 251 MHz to 500 MHz (F1), 501 MHz to 1000 MHz (F2) and 1001 MHz to 1500 MHz (F3). The frequency range of

below 250 MHz was excluded because it was more sensitive to noise. The number of distribution ranges is classified into 3 criterions in Fig. 3.11; 'full ranges', 'two ranges', and 'one range' depending on the ranges of measured frequency spectrum. For example, if the frequency spectrum is distributed in F1, F2, and F3 ranges, it corresponds to 'full ranges' as shown in Fig. 3.11 (a). If the frequency spectrum is distributed in F2 and F3 ranges, it corresponds to 'two ranges' in Fig. 3.11 (b), and if the frequency spectrum is distributed in F2 range, it corresponds to 'one ranges' in Fig. 3.11 (c). In case of Fig. 3.11 (c), the number of distribution ranges are 'full ranges' but if frequency ranges of A, C and D in Fig. 3.12 are excluded, the number of distribution ranges is 'one range' of B. The A, C, and D are an example of frequency ranges of external noise measured shortly before Fig. 3.11 (c) and these frequency ranges can be excluded by the noise-masking technique as like hatched areas of A, C, and D.

b) Maximum value

The magnitude of frequency spectrum is expressed in terms of dBm. The maximum values were divided into 3 criterions; '-30 dBm or more', 'from -44 to -31 dBm', and '-45 dBm or less'. In Fig. 3.13 (a), the maximum value is about -9 dBm in the F1 range, then '-30 dBm or more' excluding frequency ranges less than 250 MHz. If the maximum value is about -31 dBm in F2 range as shown in Fig. 3.13 (b), it corresponds to 'from -44 to -31 dBm'. If the maximum value is about -48 dBm in F3 range in Fig. 3.13 (c), it is '-45 dBm or less' excluding the noise-masking areas.
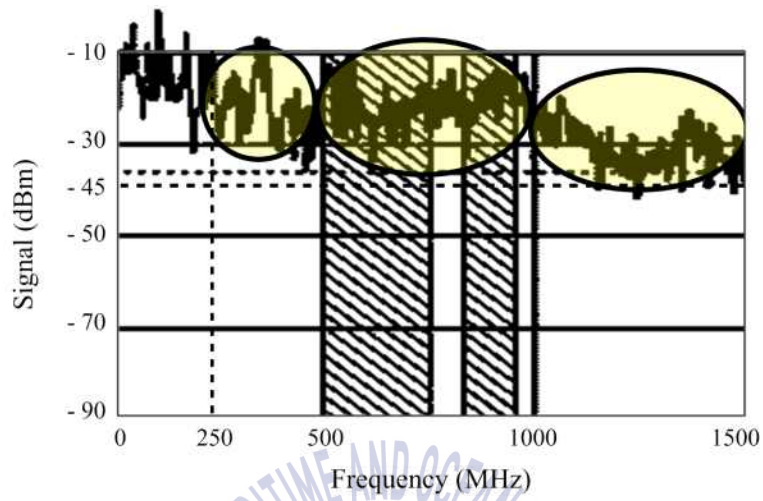
(a) Full ranges
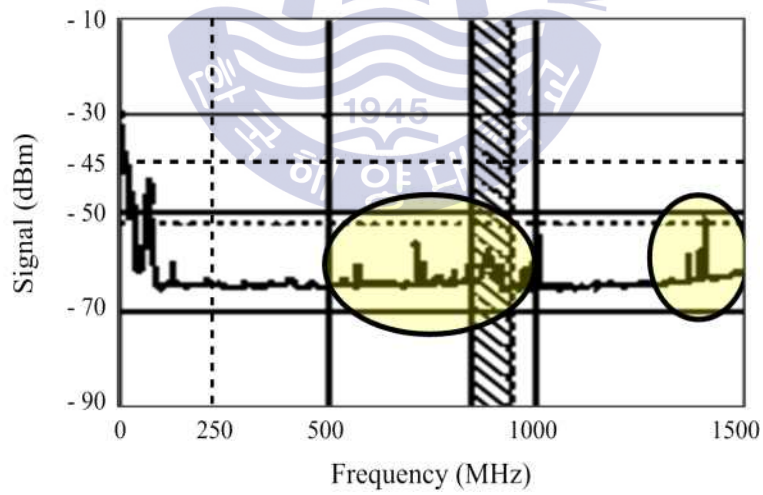
(b) Two ranges
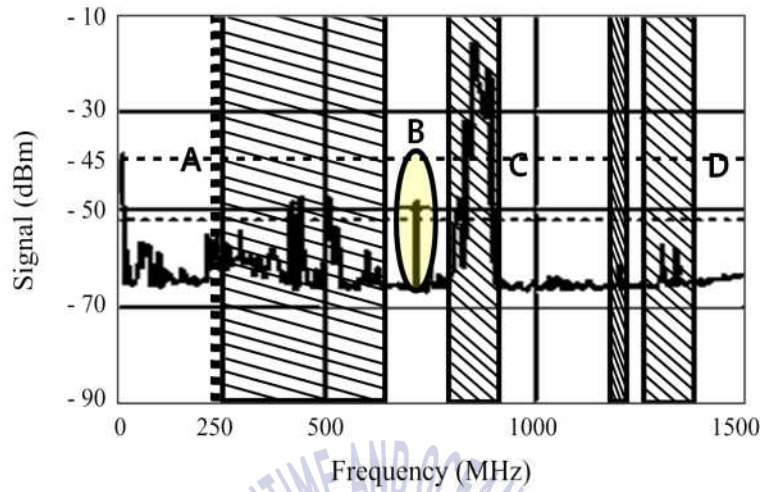
(c) One range

Fig. 3.11 The number of distribution ranges
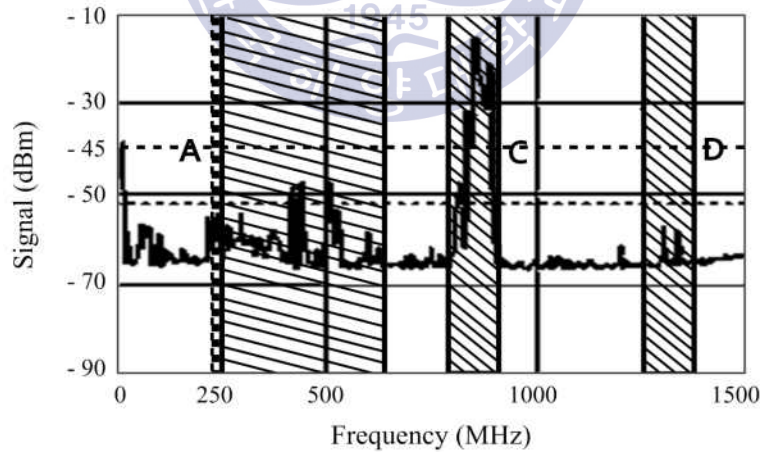
Fig. 3.12 An external noise compared with Fig. 3.11 (c)
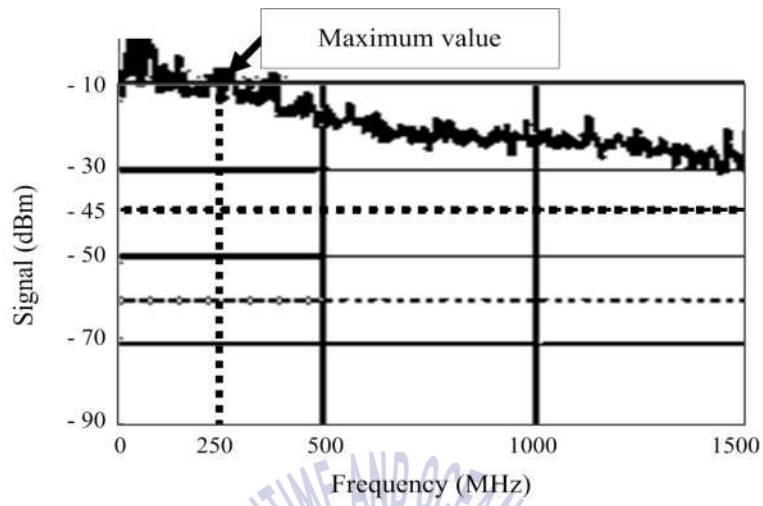
(a) -30 dBm or more
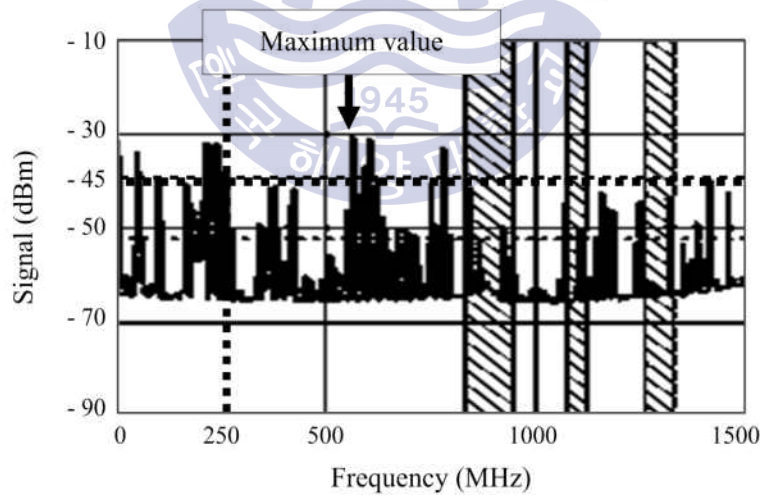
(b) From -44 to -31 dBm
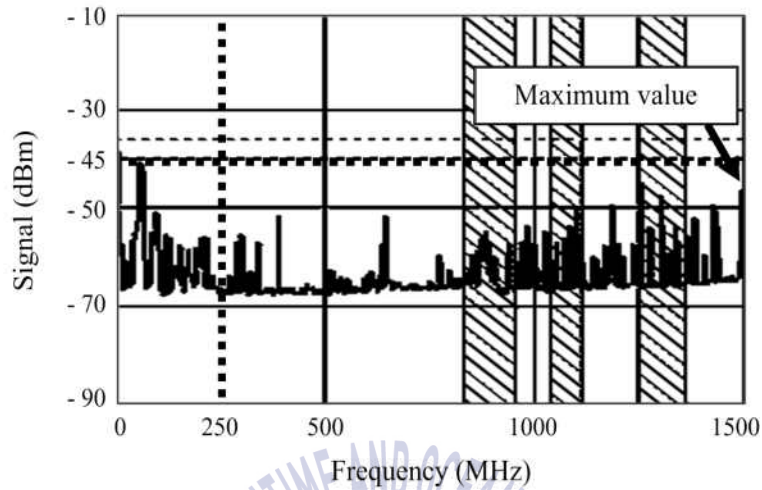
(c) -45 dBm or less

Fig. 3.13 Maximum value

c) Ranges of first and second peak values

The ranges of first and second peak values were defined as: 'F1', 'F2', and 'F3' ranges. The range of first peak value was one of three frequency ranges including the largest value and the range of second peak value was one of two frequency ranges including the largest value, excluding the range of the first peak value. For example, Fig. 3.14 shows an example of first and second peak values. Each first and second peak value corresponds respectively 'F1' and 'F2' in Fig. 3.14 (a), 'F2' and 'F3' in Fig. 3.14 (b) and 'F3' and 'F1' in Fig. 3.14 (c).
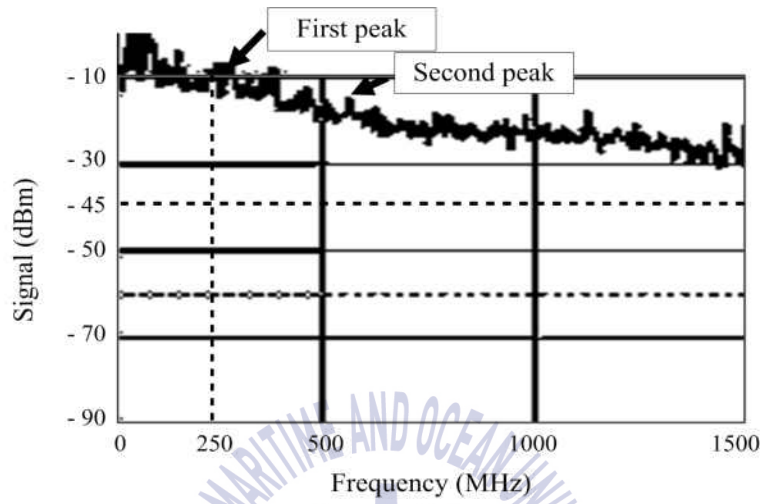
(a) F1 and F2
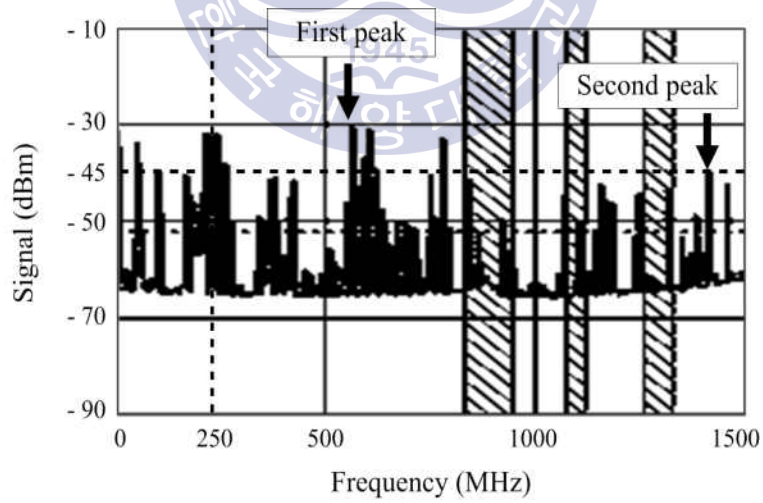
(b) F2 and F3
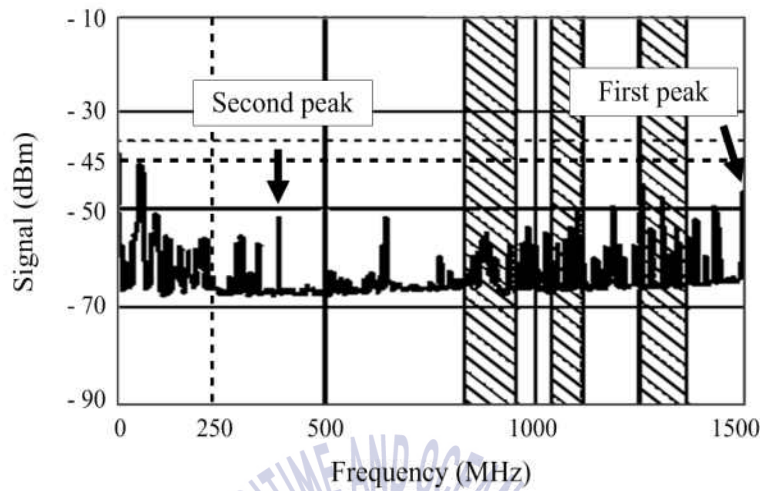
(c) F3 and F1

Fig. 3.14 First and second peak values

d) Peak differences between first and second values

Peak differences between first and second values were classified into 2 criterions; '-20 dBm or more' and 'less than -20 dBm'. Fig. 3.15 shows an example of the peak differences between first and second values, estimated respectively about -25 dBm and -6 dBm. Thus, Fig. 3.15 (a) is '-20 dBm or more' and Fig. 3.15 (b) is 'less than -20 dBm'.

e) Density levels

Depending on the frequency ranges of F1, F2, and F3, density levels of frequency spectrum were divided into 4 criterions; 'high', 'middle', 'low', and 'none'. The 'high' and 'middle' levels meant the extent to which the pulse signals were filled in all ranges and to which 4 pulse signals or more were detected in the range, respectively. The low level meant the extent to which less than 4 pulse signals were detected in the range and none meant no signals in the range. The number of pulses was counted when the pulse magnitude was over threshold excluding the noise-masking areas. Fig. 3.16 shows an example of density levels. If the pulse signals are constantly filled without any interruption in the F1 range and number of the signals is 4 pulses in the F2 range and 6 pulses in the F3 range as shown in Fig. 3.16 (a), the density levels correspond respectively 'high' in the F1 range, 'middle' in the F2 range, and 'middle' in the F3 range. If the pulse signal is only one in the F2 range and there are no pulse signals in the F1 and F3 ranges in Fig. 3.16 (b), the density levels correspond respectively 'none' in the F1 range, 'low' in the F2 range, and 'none' in the F3 range.
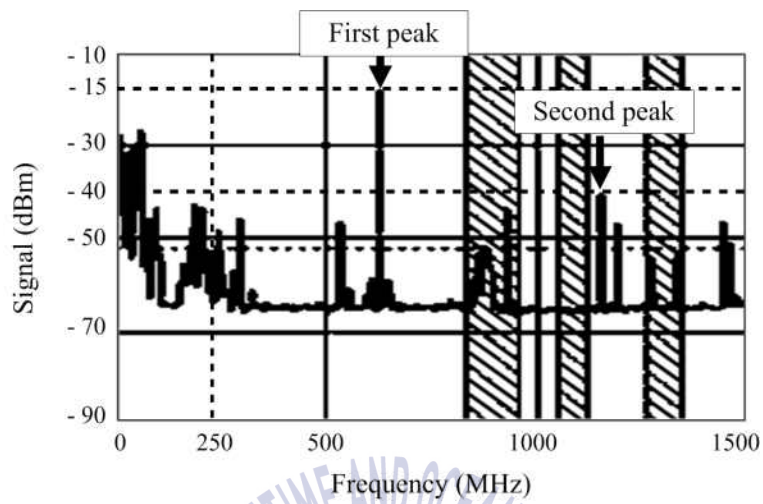
(a) -20 dBm or more
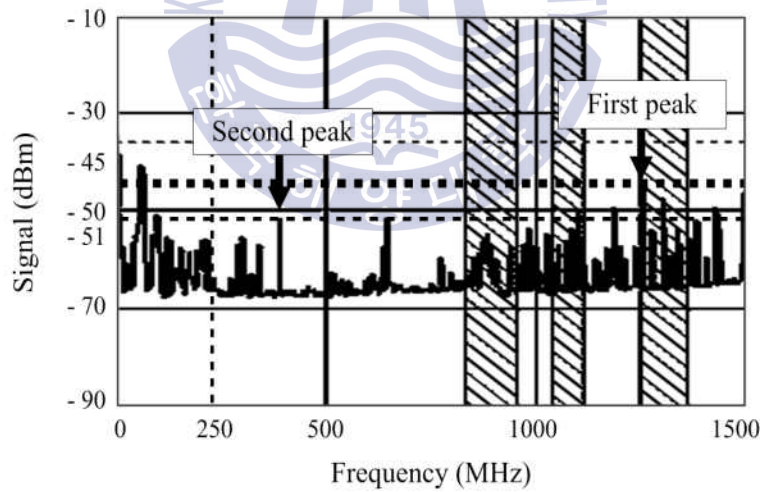
(b) Less than -20 dBm

Fig. 3.15 Peak differences
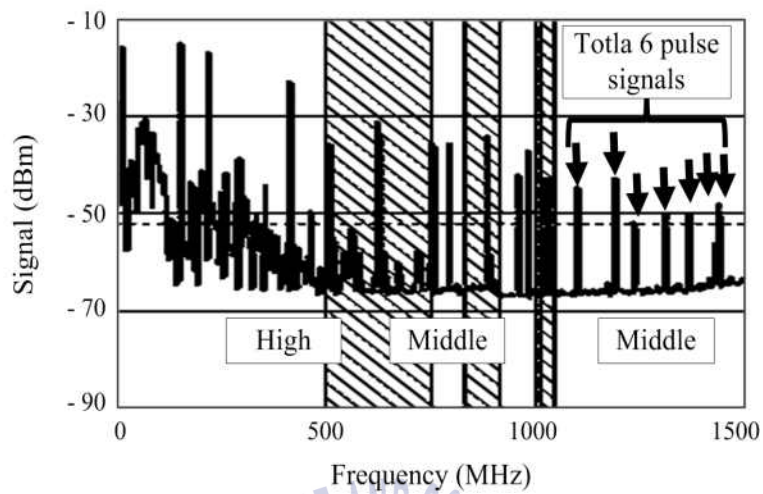
(a) High and middle
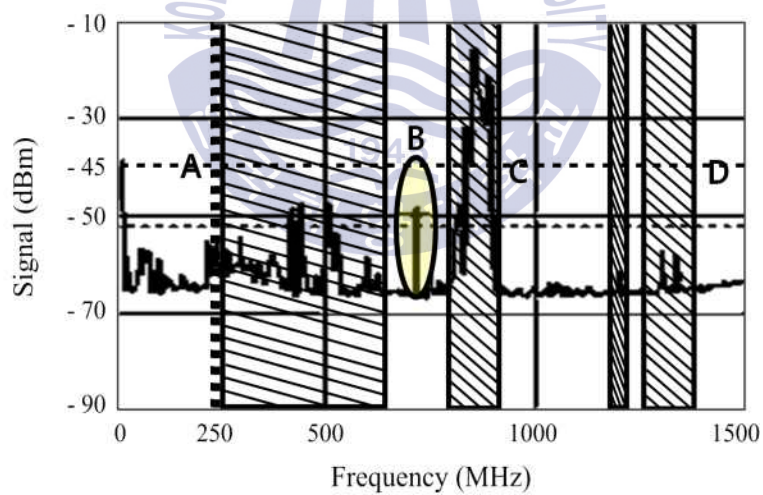
(b) Low and none

Fig. 3.16 Density levels

3.2.2 Criterions of phase parameters

a) The number of groups

The number of groups was classified into 3 criterions; 'three or more groups', 'two groups', and 'one group' depending on the groups of measured phase spectrum from 0 ˚ to 360 ˚. When the phase interval between groups was more than 20 ˚, the groups were determined as a separated group. Fig. 3.17 shows an example of the number of groups in the phase spectrum.

b) Overall distribution ranges or not

This parameter was divided by 2 criterions; 'Overall ranges' and 'Not overall ranges'. Fig. 3.18 shows an example of overall distribution ranges or not. If the signal distribution of phase spectrum is generated in overall ranges, it corresponds to 'overall ranges' in Fig. 3.18 (a) and if not, it means 'not overall ranges' in Fig. 3.18 (b).
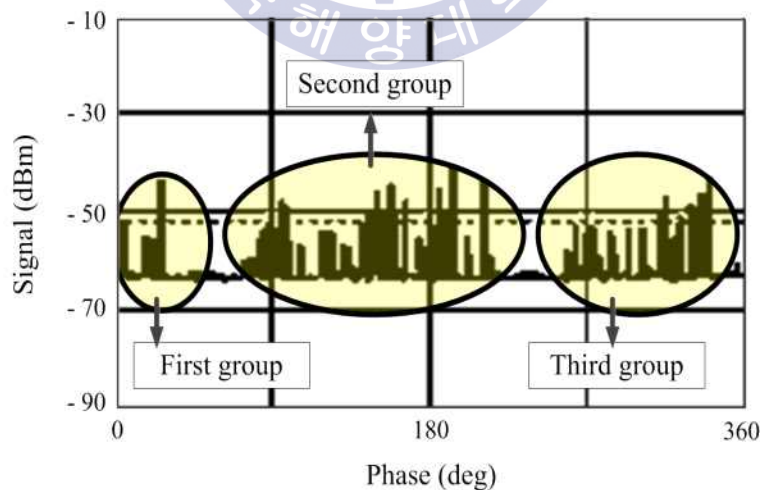
(a) Three or more groups
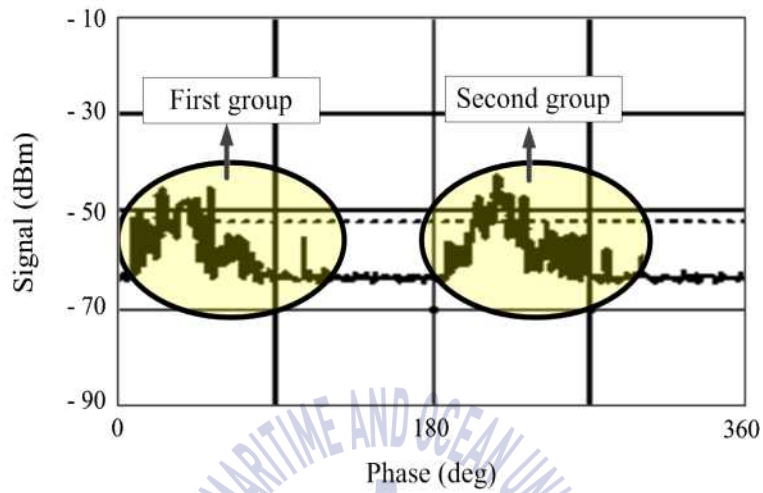
(b) Two groups
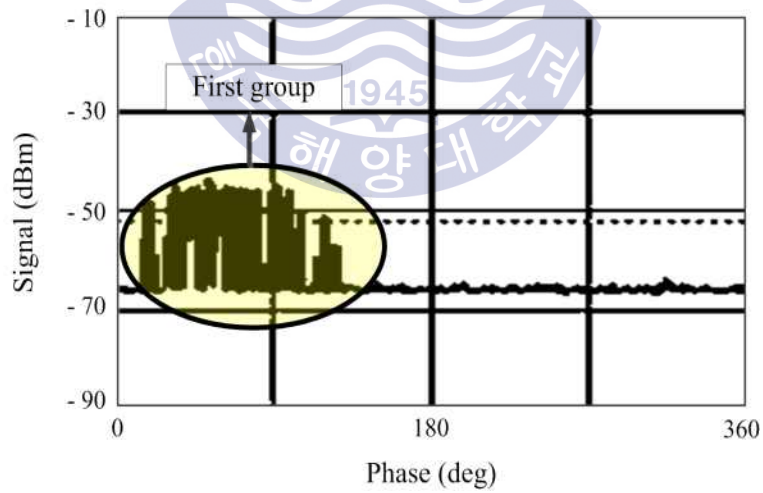
(c) One group

Fig. 3.17 The number of groups
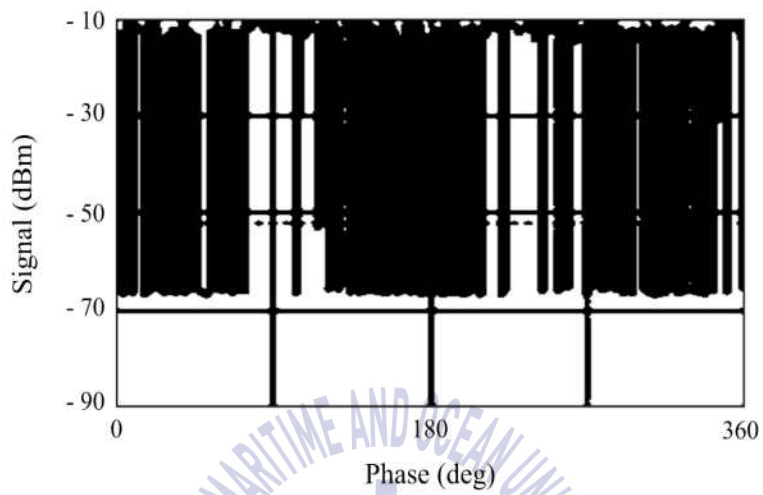
(a) Overall ranges
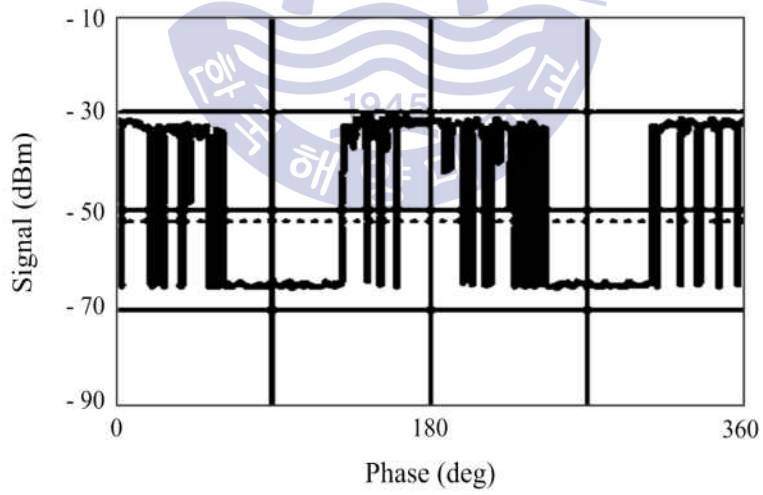
(b) Not overall ranges

Fig. 3.18 Overall distribution ranges or not

c) Distribution ranges of each group

Depending on the each group, the distribution ranges were classified into 3 criterions; '90° or more', 'less than 90°, and 'none'. Fig. 3.19 shows an example of distribution ranges of each group. If each distribution range of first and second groups is more than 90°, first and second groups correspond to '90° or more' each in Fig. 3.19 (a). If there is only the first group and distribution range of first group is below 90°, first and second groups correspond 'less than 90°' and 'none', respectively, as shown in Fig. 3.19 (b). If there are no groups in the phase spectrum, all of the first and second groups are 'none' in Fig 3.19 (c).
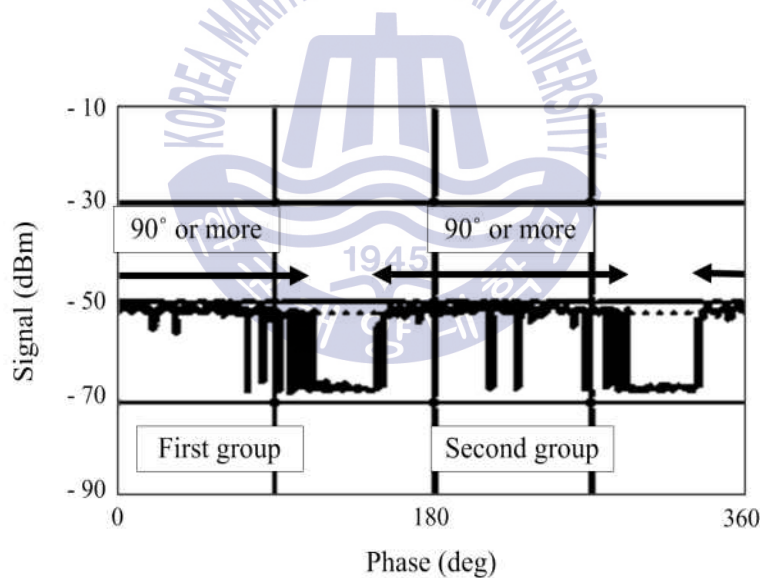
(a) 90° or more
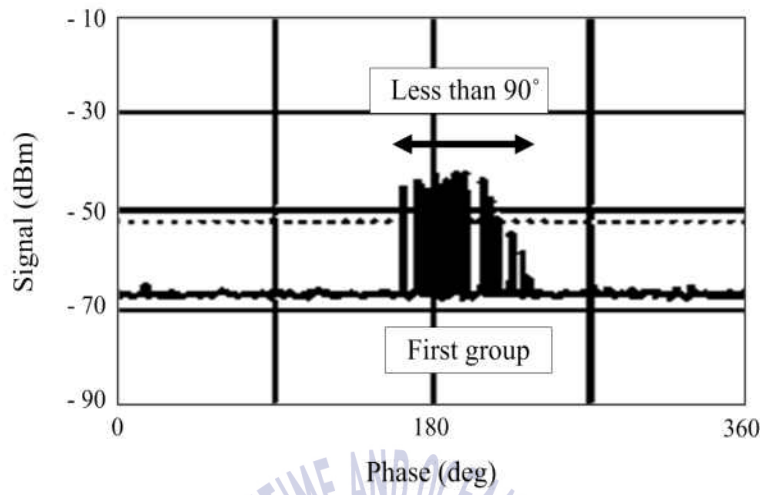
(b) Less than 90°
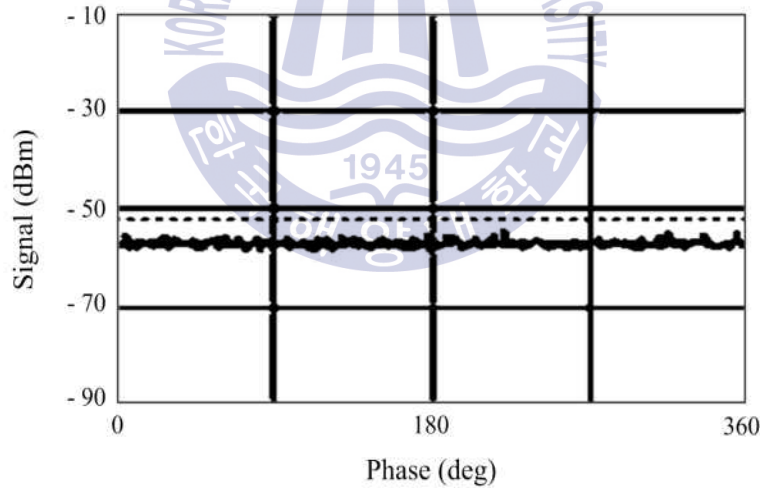
(c) None

Fig. 3.19 Distribution ranges of each group

d) Density levels

Depending on the distribution ranges of first and second groups, density levels of phase spectrum were divided into 4 criterions; 'high', 'middle', 'low', and 'none'. The 'high' and 'middle' levels meant the extent to which the pulse signals were filled in all ranges and to which 4 pulse signals or more were detected in the range, respectively. The low level meant the extent to which less than 4 pulse signals were detected in the range and none meant no signals in the range. The number of pulses was counted when the pulse magnitude was over threshold. Fig. 3.20 shows an example of density levels. If the pulse signals are constantly filled without any interruption in all of the first and second groups, the density levels are 'high' in the first and second group in Fig 3.20 (a). If the phase signals are more than 4 pulses in the first group and 3 pulses in the second group, the density levels correspond to 'middle' and 'low' in Fig. 3.20 (b). If there are no groups, it is 'none'. The reason why the first and second groups are reversed in Fig. 3.20 (a) is defined that the group occurring at 0 ˚ is as the first group.

e) Peak differences between first and second groups

Peak differences between first and second groups were classified into 2 criterions; '-10 dBm or more' and 'less than -10 dBm'. Fig. 3.21 shows an example of the peak differences between first and second groups. If the peak difference between first and second groups is about -15 dBm, it corresponds to '-10 dBm or more' in Fig. 3.21 (a) and there is little peak difference between first and second groups, it corresponds to 'less than -10 dBm' in Fig. 3.21 (b).
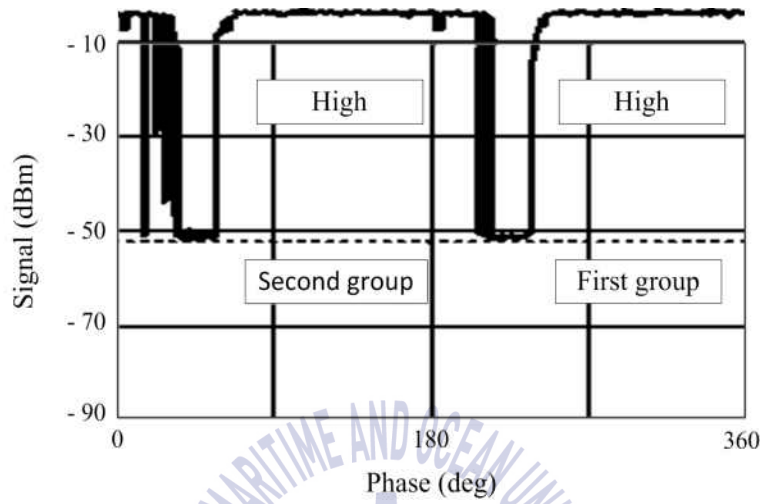
(a) High and high
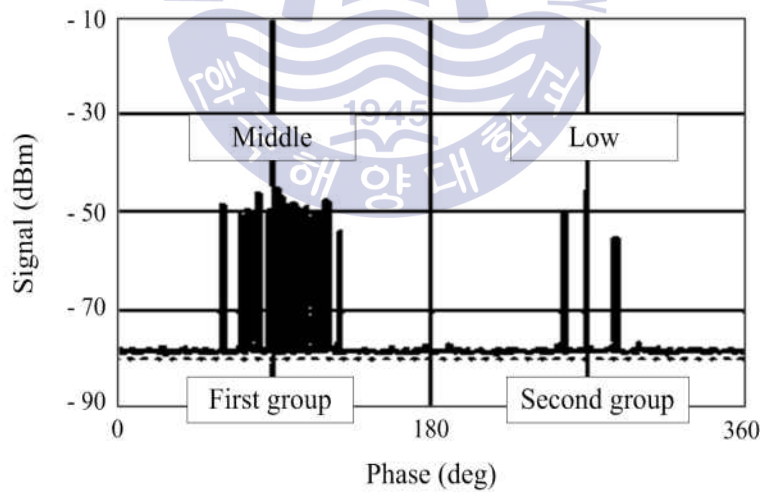
(b) Middle and low

Fig. 3.20 Density levels
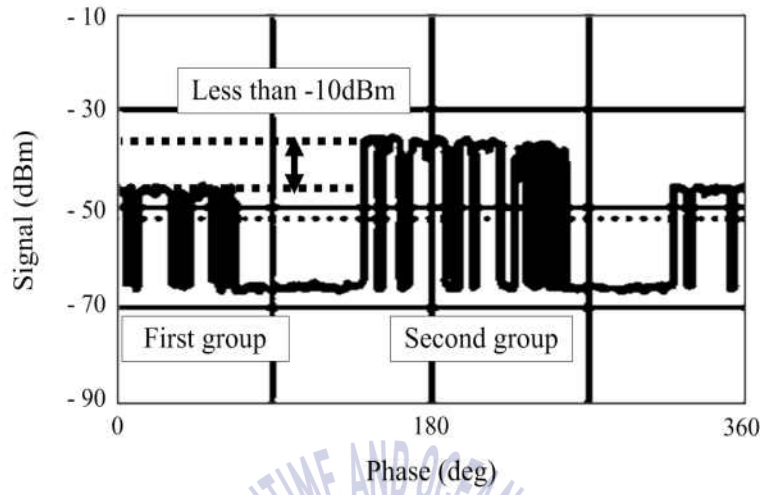
(a) -10 dBm or more
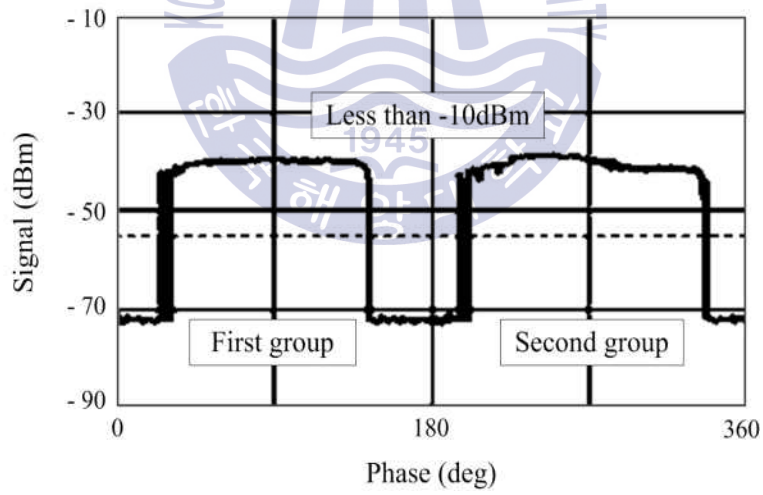
(b) Less than -10 dBm

Fig. 3.21 Peak differences between groups

f) Shapes

Based on the representative data, the phase shapes were classified into 13 criterions for each group. The 13 phase shapes were defined as shape 1 to 13. Fig. 3.22 shows the shapes of actual phase spectrum measured in the field and normalized phase spectrum.

(a) Shape 1

(b) Shape 2
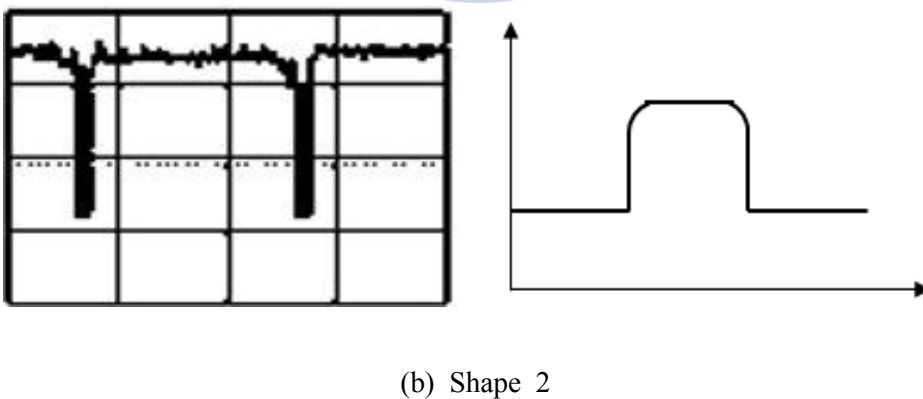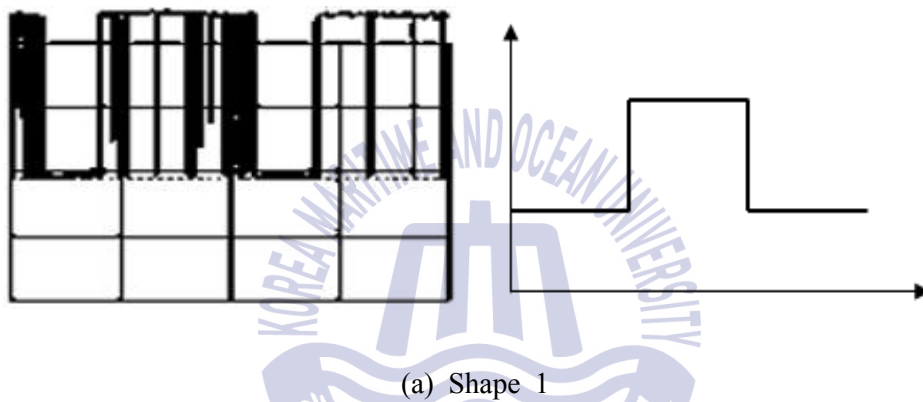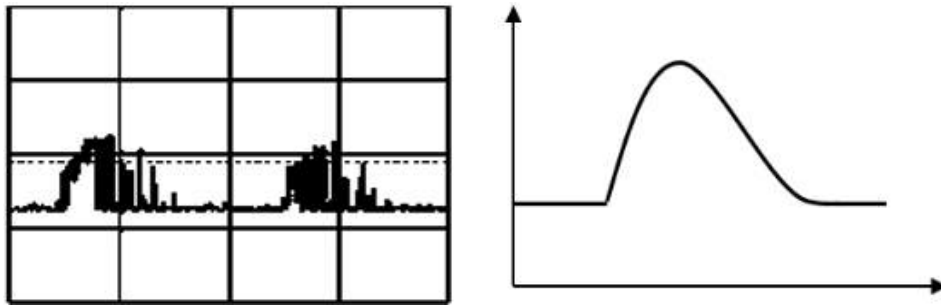
(c) Shape 3
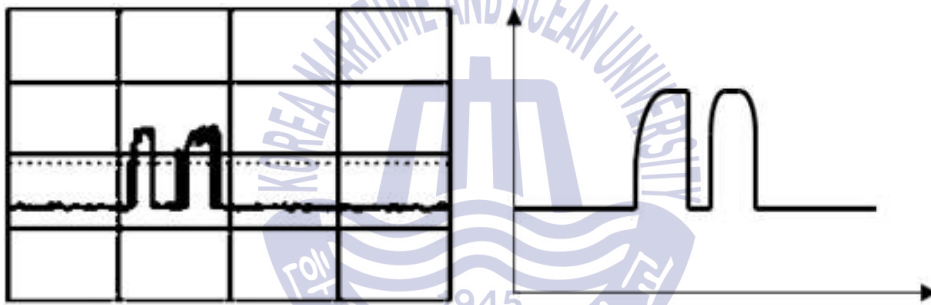
(d) Shape 4
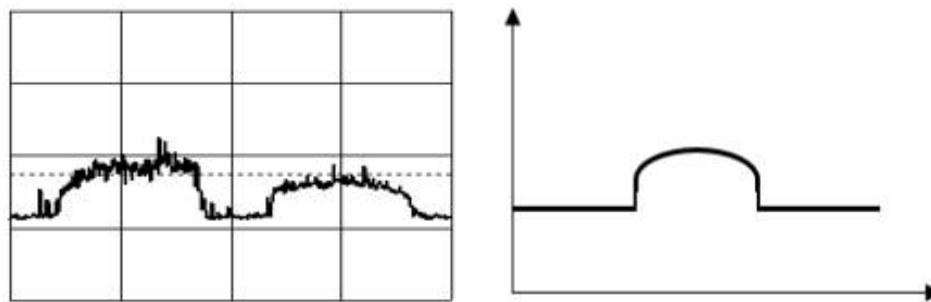
(e) Shape 5
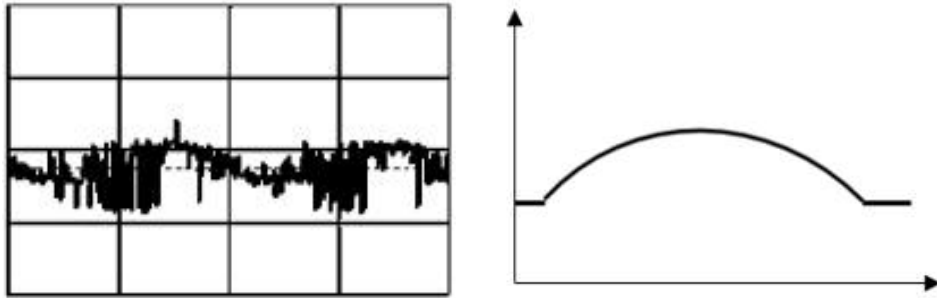
(f) Shape 6
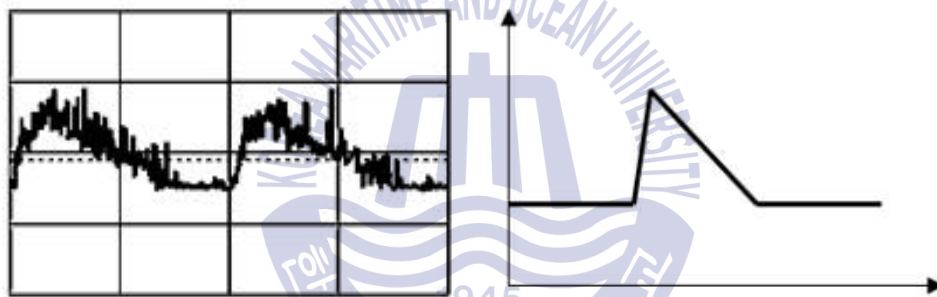
(g) Shape 7
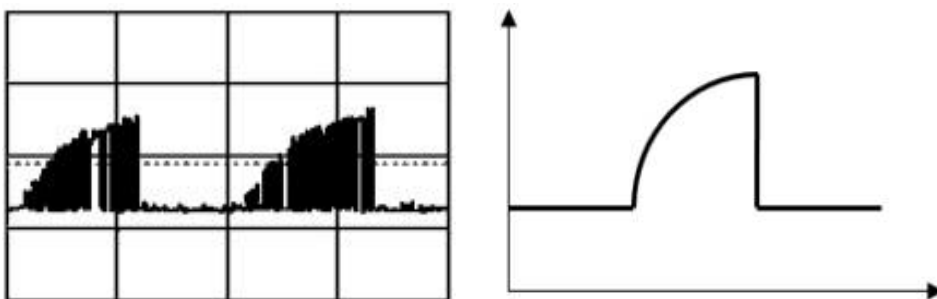
(h) Shape 8
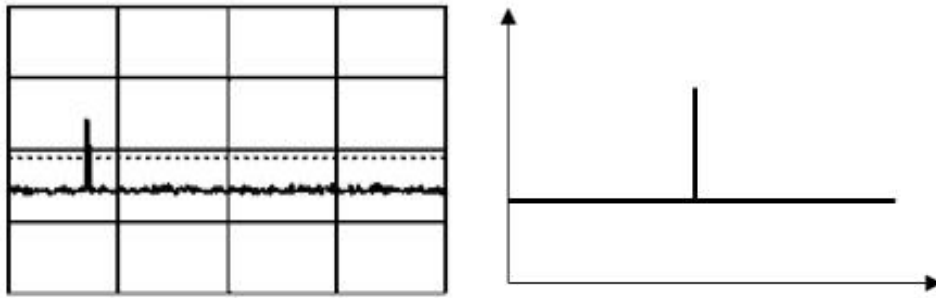
(i) Shape 9
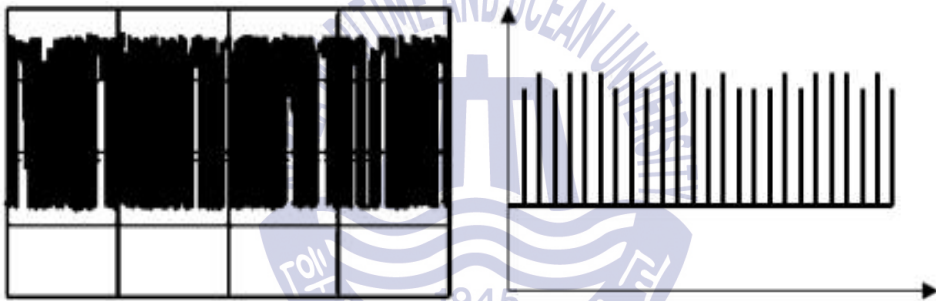
(j) Shape 10
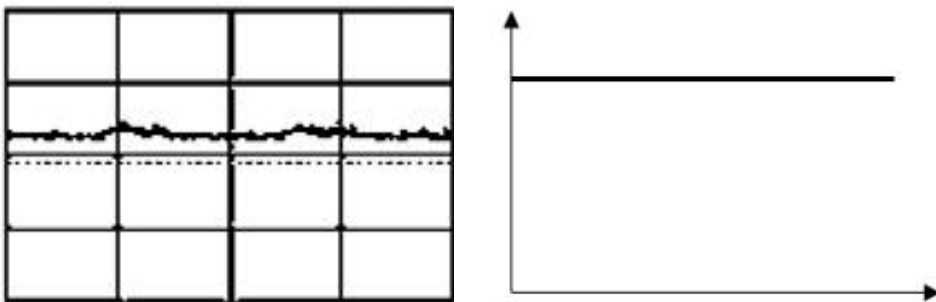
(k) Shape 11
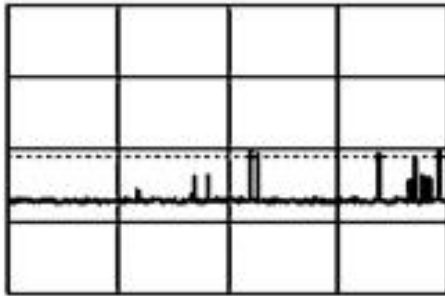
The pattern is unclear

(l) Shape 12
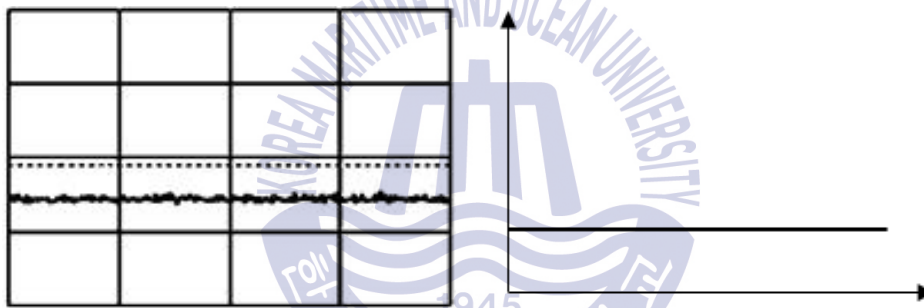
(m) Shape 13

Fig. 3.22 Shapes of actual and normalized phase spectrum

Table 3.3 and Table 3.4 show the criterions of features including 5 frequency parameters such as the number of distribution ranges, maximum value, frequency ranges of first and second peak values, peak differences between first and second values and density levels, and 6 phase parameters including the number of phase groups, overall distribution ranges or not, distribution ranges of each group, density levels, peak differences between the first and second groups, and shapes.

Table 3.3 Criterions of 6 frequency parameters

Frequency parameters	Criterions		
The number of distribution ranges	Full ranges		
	Two ranges		
	One range		
Maximum value	-30 dBm or more		
	from -44 to -31 dBm		
	-45 dBm or less		
Ranges of first and second peak value	First peak value		F1
			F2
			F3
	Second peak value		F1
			F2
			F3
Peak differences between first and second value	-20 dBm or more		
	less than -20 dBm		
Density levels	F1		High
			Middle
			Low
			None
	F2		High
			Middle
			Low
			None
	F3		High
			Middle
			Low
			None

Table 3.4 Criterions of 5 phase parameters

Phase parameters	Criterions		
The number of groups	One groups		
	Two groups		
	Three or more groups		
Overall distribution ranges or not	Overall ranges		
	Not overall ranges		
Distribution ranges of each group	First group	90° or more	
		Less than 90°	
		None	
	Second group	90° or more	
		Less than 90°	
		None	
Density levels	Frist group	High	
		Middle	
		Low	
		None	
	Second group	High	
		Middle	
		Low	
		None	
Peak Differences between first group and second group	Less than -10 dBm		
	-10 dBm or more		
Shapes	First group	Shape 1 to 13	
	Second group	Shape 1 to 13	

3.2.3 Effective feature parameters

Depending on the criterions of 5 frequency and 6 phase parameters, 82 cases of the representative data were classified as shown in Table 3.5 and

Table 3.6. The feature analysis was performed according to defects including types of 6 PDs and 4 noises. Table 3.7 and Table 3.8 show the analysis of the effective frequency and phase parameters according to defects. The 6 PDs and 4 noises were defined as type A to F of PDs and type A to D of noises, respectively.

Table 3.5 An example of data classification by the frequency parameters

Frequency parameters	Criterions		Reference data No.			
			1	2	2	4
The number of distribution ranges	Full ranges		●	●	●	●
	Two ranges					
	One range					
Maximum value	-30 dBm or more			●	●	●
	from -44 to -31 dBm		●			
	-45 dBm or less					
Ranges of first and second peak value	First peak value	F1	●	●	●	●
		F2				
		F3				
	Second peak value	F1				
		F2	●	●	●	●
		F3				
Peak differences	-20 dBm or more					
	less than -20 dBm		●	●	●	●
Density levels	F1	High			●	●
		Middle	●	●		
		Low				
		None				
	F2	High	●		●	●
		Middle		●		
		Low				
		None				
	F3	High			●	●
		Middle		●		
		Low	●			
		None				

Table 3.6 An example of the data classification by the phase parameters

Phase parameters	Criterions		Reference data No. 1	2	3	4
The number of groups	One groups		●			
	Two groups			●	●	●
	Three or more groups					
Overall distribution ranges or not	Overall ranges					
	Not overall ranges		●	●	●	●
Distribution ranges of each group	First group	90 ˚ or more		●		●
		Less than 90 ˚	●		●	
		None				
	Second group	90 ˚ or more		●		●
		Less than 90 ˚			●	
		None	●			
Density levels	Frist group	High		●	●	●
		Middle	●			
		Low				
		None				
	Second group	High		●	●	●
		Middle				
		Low				
		None	●			
Peak Differences between first group and second group	Less than -10 dBm		●	●	●	●
	-10 dBm or more					
Shapes	First group	Shape 1 to 13	Shape 2	Shape 1	Shape 4	Shape 5
	Second group	Shape 1 to 13	Shape 13	Shape 1	Shape 4	Shape 5

Table 3.7 Effective frequency parameters according to defects

Information		Defect Classification	Partial Discharge						External Noise			
		Defect types	A	B	C	D	E	F	A	B	C	D
		Total [%]	100	100	100	100	100	100	100	100	100	100
Frequency	The number of distribution ranges	Full ranges	100	73	78	50	0	0	100	25	100	0
		Two ranges	0	20	22	0	100	0	0	25	0	100
		One range	0	7	0	50	0	100	0	50	0	0
	Maximum value	-30 dBm or more	84	13	33	0	0	0	60	0	100	100
		from -44 to -31 dBm	13	47	44	0	0	0	40	25	0	0
		-45 dBm or less	3	40	22	100	100	100	0	75	0	0
	Ranges of first and second peak value	First peak value F1	42	33	11	0	0	0	60	25	0	0
		First peak value F2	45	33	56	50	0	100	40	75	100	100
		First peak value F3	13	33	33	50	100	0	0	0	0	0
		Second peak value F1	18	0	56	0	0	0	40	25	17	100
		Second peak value F2	55	60	33	0	100	0	60	25	0	0
		Second peak value F3	26	33	11	50	0	0	0	0	83	0
	Peak differences between first and second value	-20 dBm or more	8	7	44	0	0	0	60	0	50	100
		less than -20 dBm	92	87	56	50	100	0	40	50	50	0
	Density levels	F1 High	63	0	56	0	0	0	60	0	67	
		F1 Middle	34	60	22	0	0	0	40	25	17	0
		F1 Low	3	20	0	50	0	0	0	25	17	100
		F1 None	0	20	22	50	100	100	20	50	0	0
		F2 High	50	0	56	0	0	0	40	0	83	0
		F2 Middle	50	80	44	50	100	0	60	25	17	0
		F2 Low	0	20	0	0	0	100	0	75	0	100
		F2 None	0	0	0	50	0		0	0	0	0
		F3 High	47	0	0	0	0	0	20	0	50	0
		F3 Middle	50	53	89	50	100	0	40	0	50	0
		F3 Low	3	33	11	50	0	0	40	25	0	0
		F3 None	0	13	0	0	0	100	0	75	0	100

Table 3.8 Effective phase parameters according to defects

Information			Partial Discharge						External Noise			
		Types	A	B	C	D	E	F	A	B	C	D
		Total [%]	100	100	100	100	100	100	100	100	100	100
Phase	The number of groups	One group	5	27	0	0	100	0	0	50	33	100
		Two groups	95	73	100	100	0	100	100	25	67	0
		Three or more groups	0	0	0	0	0	0	0	25	0	0
	Overall distribution or not	Overall ranges	0	0	0	0	100	0	0	25	33	0
		Not overall ranges	100	100	100	100	0	100	100	75	67	100
	Distribution ranges of each group	First group 90° or more	71	60	100	50	100	0	80	50	100	100
		First group Less than 90°	29	40	0	50	0	100	20	50	0	0
		First group None	0	0	0	0	0	0	0	0	0	0
		Second group 90° or more	66	40	100	50	0	100	80	25	67	0
		Second group Less than 90°	29	33	0	50	0	0	20	25	0	0
		Second group None	5	27	0	0	100	0	0	50	33	100
	Density levels	First group High	63	0	89	100	100	100	40	25	67	100
		First group Middle	37	100	11	0	0	0	60	50	33	0
		First group Low	0	0	0	0	0	0	0	25	0	0
		First group None	0	0	0	0	0	0	0	0	0	0
		Second group High	66	7	89	100	0	0	60	0	33	0
		Second group Middle	26	67	11	0	0	100	40	50	33	0
		Second group Low	3	0	0	0	0	0	0	0	0	0
		Second group None	5	27	0	0	100	0	0	50	33	100
	Peak differences	Less than -10 dBm	95	73	100	100	0	100	80	50	67	0
		-10 dBm or more	94	27	0	0	100	0	20	50	33	100
	Shapes	First group Shape 1	79	0	11	0	0	100	60	0	17	100
		First group Shape 2	21	0	0	0	0	0	20	0	50	0
		First group Shape 3	0	93	0	0	0	0	0	0	0	0
		First group Shape 4	0	7	0	0	0	0	0	0	0	0
		First group Shape 5	0	0	0	100	0	0	0	0	0	0
		First group Shape 6	0	0	0	0	100	0	0	0	0	0
		First group Shape 7	0	0	44	0	0	0	0	0	0	0
		First group Shape 8	0	0	44	0	0	0	0	0	0	0
		First group Shape 9	0	0	0	0	0	0	0	25	0	0
		First group Shape 10	0	0	0	0	0	0	0	0	33	0
		First group Shape 11	0	0	0	0	0	0	0	25	0	0
		First group Shape 12	0	0	0	0	0	0	20	50	0	0
		Second group Shape 1	76	0	11	0	0	100	60	0	17	0
		Second group Shape 2	18	0	0	0	0	0	0	0	50	0
		Second group Shape 3	0	73	0	0	0	0	0	0	0	0
		Second group Shape 5	0	0	0	100	0	0	20	0	0	0
		Second group Shape 7	0	0	44	0	0	0	0	0	0	0
		Second group Shape 8	0	0	44	0	0	0	0	0	0	0
		Second group Shape 12	0	0	0	0	0	0	20	50	0	0
		Second group Shape 13	5	27	0	0	100	0	0	50	33	100

From the result of feature analysis, 5 of 11 frequency and phase parameters were effective to classify types of 6 PDs and 4 noises clearly based on the decision tree method using the representative data of 82 cases. The 5 effective parameters are defined as following.

a) Phase - the number of groups (first step)

The number of phase groups was used to distinguish the case of noise(Type B) more than three phase groups in Table 3.9. From the first step, 1 of 82 cases could be distinguished using the criterion of 'three or more', as shown in Table 3.9. As a result, less than 1% of the total representative data could be classified.

Table 3.9 Classification of the representative data in the first step

First step	Defects	Data classification
Three or more groups	Noise	1
Two groups	PDs and Noises	69
One group	PDs and Noises	12
Total data		82

b) Phase - shapes (second step)

The remaining representative data of 81 cases including 66 PDs and 15 noises were classified by the phase shapes for each group in Table 3.10. From the second step, 32 of 81 cases could be distinguished using the criterions, as shown in Table 3.10. As a result, about 40 % of the total representative data could be classified.

Table 3.10 Classification of the representative data in the second step

First step	Second step		Types of defects		Data classification
	First group	Second group	Defects	Types	
Two groups	Shape 1	Shape 1	PD	A	30
				C	1
				F	1
			Noise	A	3
				C	1
	Shape 2	Shape 2	PD	A	6
			Noise	C	3
	Shape 2	Shape 5	Noise	A	1
	Shape 3	Shape 3	PD	B	11
	Shape 5	Shape 5	PD	D	2
	Shape 7	Shape 7	PD	C	4
	Shape 8	Shape 8	PD	C	4
	Shape 12	Shape 12	Noise	A	1
			Noise	B	1
One group	Shape 1	Shape 13	PD	A	1
			Noise	D	1
	Shape 2	Shape 13	PD	A	1
	Shape 3	Shape 13	PD	B	3
	Shape 4	Shape 13	PD	B	1
	Shape 6	Shape 13	PD	E	1
	Shape 9	Shape 13	Noise	B	1
	Shape 10	Shape 13	Noise	C	2
	Shape 11	Shape 13	Noise	B	1
Total data					81

c) Frequency – The number of distribution ranges & density levels (third step)

   The remaining representative data of 49 cases including 39 PDs and 10 noises were classified by the number of distribution ranges & the density

- 81 -

levels. From the third step, 35 of 49 cases could be distinguished using the criterions, as shown in Table 3.11.

Table 3.11 Classification of the representative data in the third step

Second step		Third step		Types of defects		Data classification
First group	Second group	The number of distribution ranges	Density levels	Defects	Types	
Shape 1	Shape 1	Full ranges	F1, F2, and F3: High or middle	PD	A	29
					C	1
				Noise	A	3
					C	1
			F1, F2, or F3: Low or none	PD	A	1
		One range	F1, F2 and F3: Low or none	PD	F	1
Shape 2	Shape 2	Full ranges	F1, F2, and F3: High or middle	PD	A	6
				Noise	C	3
Shape 12	Shape 12	Full ranges	-	Noise	A	1
		One range	-	Noise	B	1
Shape 1	Shape 13	Full ranges	F1, F2, and F3: High or middle	PD	A	1
		Two range	F1, F2, or F3: Low or none	Noise	D	1
Total data						49

As a result, about 42 % of the total representative data could be classified. The 6 cases of PDs (type A) and 3 cases of noises (type C) could be

classified by the next step but other 5 cases including a PD (type C) and 4 noise cases (types of A and C) could not be distinguished using any other parameters.

d) Frequency - ranges of first and second peak values (fourth step)

The ranges of first and second peak values were used to classify type A of PDs and type C of noises. From the fourth step, all of the 9 cases could be distinguished using the criterions, as shown in Table 3.12. As a result, about 11% of the total representative data could be classified.

Table 3.12 Classification of the representative data in the fourth step

Third step		Fourth step		Types of defects		Data classification
The number of distribution ranges	Density levels	first peak	second peak	Defects	Types	
Full ranges	F1, F2 and F3: High or middle	F1	F2	PD	A	6
		F2	F1			
		F3	F2			
		F2	F3	Noise	C	3
Total data						9

Chapter 4 New Method of PD Diagnosis

4.1 New PD diagnostic algorithm

To develop new method of PD diagnosis without the phase synchronization, the 5 effective parameters of 11 frequency and phase parameters were selected by analyzing 82 cases of the representative data. From the result, the new algorithm can classify 6 types of PDs and 4 types of noises clearly in Fig. 4.1, based on the decision tree technique step by step; the number of groups in phase parameters, shapes in phase parameters, the number of distribution ranges & density levels in frequency parameters, and ranges of first and second peak value in frequency parameters.

In order to evaluate the new method for PD diagnosis proposed in this thesis, the diagnosis result was compared with that of the conventional method using 82 cases of representative data, with the results presented in Table 4.1. The accuracy rate of conventional method was much lower than that of the new method which was about 94% because the conventional method could not classify types of defects clearly using the phase-asynchronous PD data, which were caused by phase absence of voltage applied to GIS during on-site PD measurement.

Table 4.1 Comparison of diagnosis performance

Method	New method	Conventional method
Principle	Decision tree	Artificial neural network
Accuracy rate %	94 (77/82)	11 (9/82)

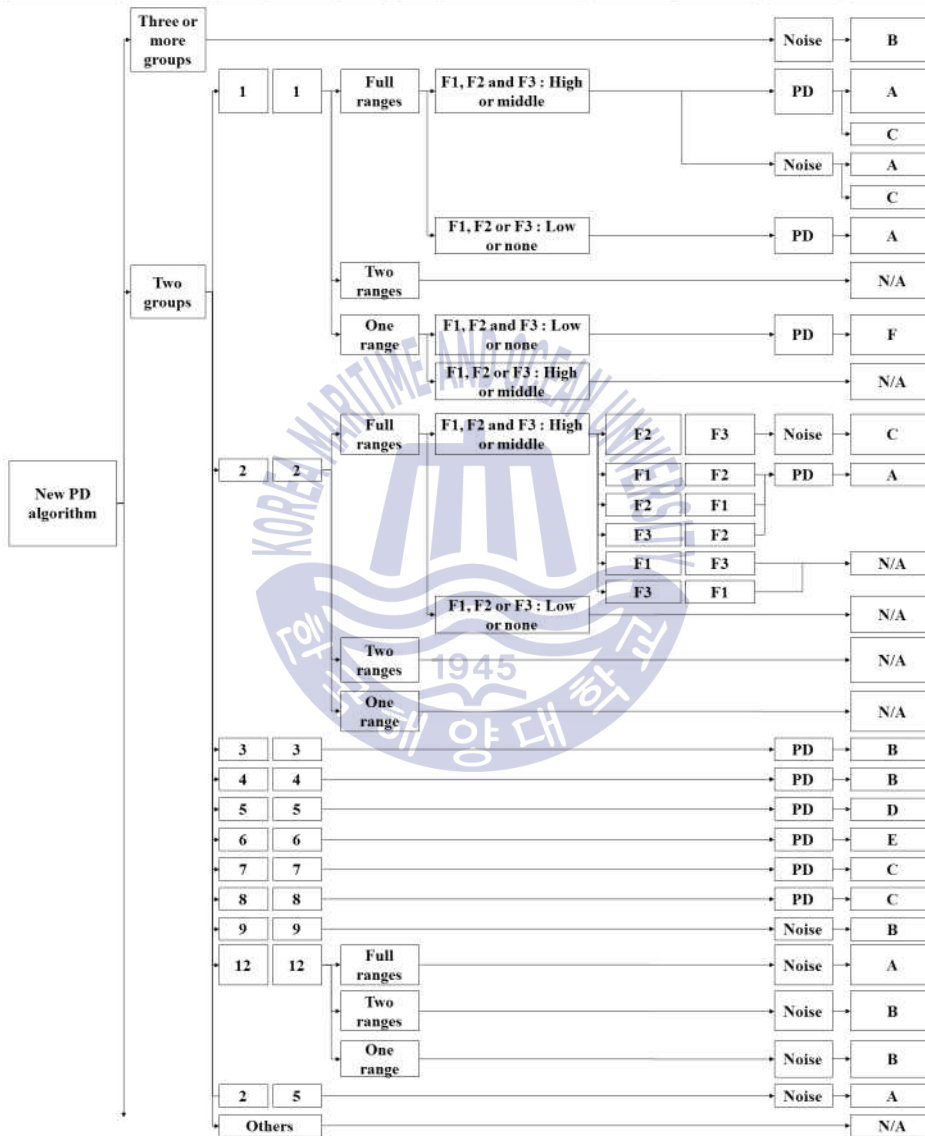| Input							Output	
Features	Phase			Frequency			Classification	
Parameters	The number of groups	Shapes		The number of distribution ranges	Density levels	Range of peak values	Defects	Types
		First	Second			First Peak / Second Peak		

Fig. 4.1 A flow chart of new method for PD diagnosis

Depending on the criterions of 5 effective parameters, the on-site engineers can classify types of defects clearly for determining GIS maintenance and repair work in the factory and the field during on-site PD measurement. Furthermore, it is a very useful tool to collect additional UHF PD data as a same type of PD database.

4.2 Case studies in Korea and Malaysia

To verify the reliability of the new method proposed in this thesis, it was applied to on-site GIS PD diagnosis in South Korea and Malaysia. The procedure of new method for on-site PD measurement by four steps as shown in Fig. 4.2.

a) Floating case in Korea

A PD occurred intermittently with abnormal sound inside one of the disconnecting switch (DS) of 362 kV GIS in Korea. The PD signal was detected by the portable UHF PD device without synchronization. The frequency and phase spectrum are shown in Fig. 4.3. They were analyzed with the conventional and new methods in the field. The on-site diagnosis results of conventional and new methods were crack in spacer and floating element, respectively. Table 4.2 shows the diagnosis result of new method for 362 kV GIS. From the result of the internal inspection by on-site engineers, it was found that a bolt and nut were not tightened properly on the cover of the DS bottom as shown in Fig. 4.4.
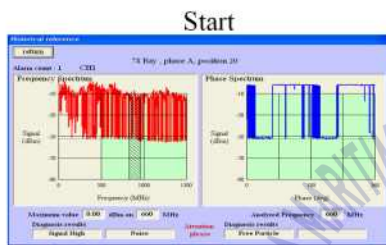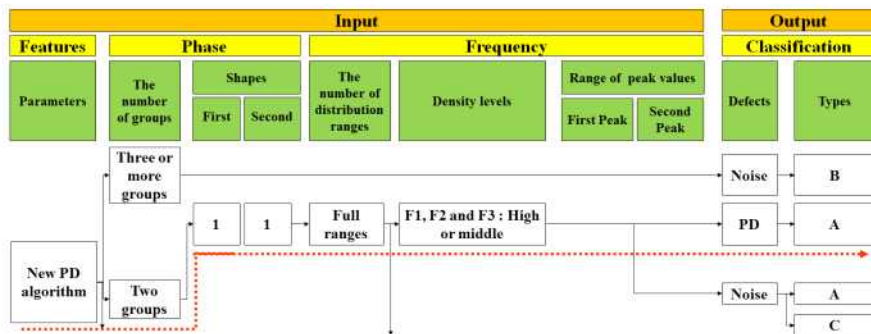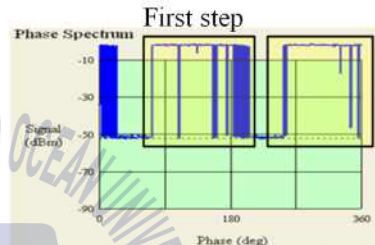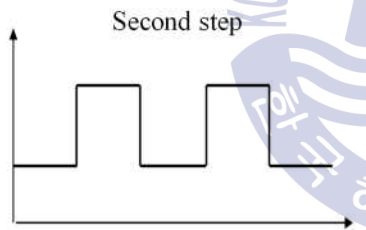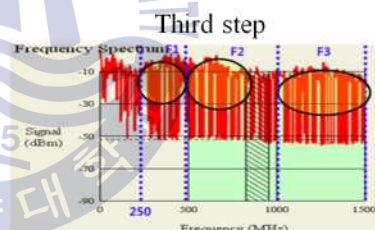
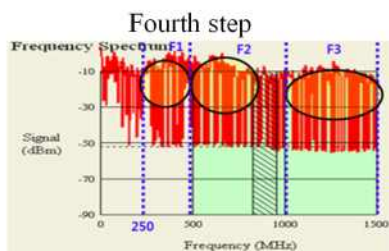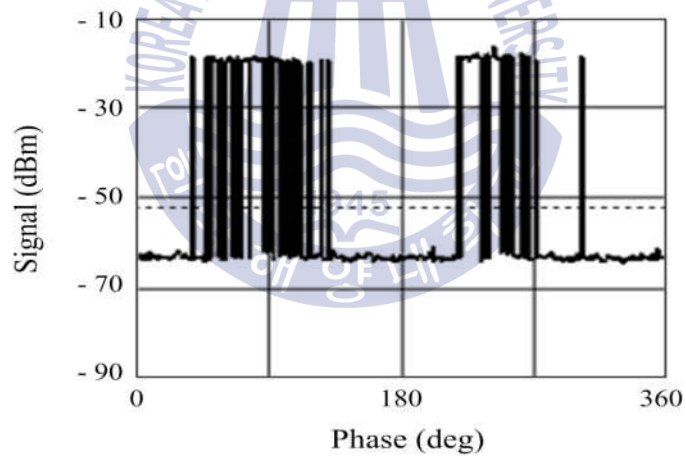Fig. 4.2 On-site application of new PD diagnostic method
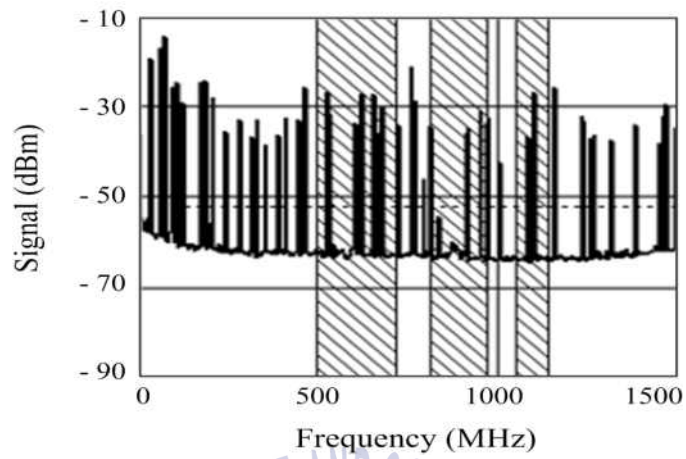
(a) Frequency spectrum

(b) Phase spectrum

Fig. 4.3 Frequency and phase spectrums measured in 362 kV GIS

Table 4.2 Diagnosis result of new method for 362 kV GIS

Diagnosis steps			New PD diagnostic algorithm
First step			Two groups
Second step	First group		Shape 1
	Second group		Shape 1
Third step	The number of distribution ranges		Full ranges
	Density levels	F1	High
		F2	High
		F3	High
Fourth step	First peak		F2
	Second peak		F1
Diagnosis result			Floating element

Fig. 4.4 Photographs of internal defect in 362 kV GIS

b) Void case in Korea

A PD was detected by the on-line UHF PD device without phase synchronization in 170 kV GIS. The PD occurred continuously and the frequency and phase spectrum are shown in Fig. 4.5. The on-site diagnosis result of conventional method was external noise. On the other hand, the diangosis result of new method was void in Table 4.3. From the result of the internal inspection by on-site engineers, it was found that a void with carbonized trace inside the insulator of main bus as shown in Fig. 4.6.

(a) Frequency spectrum
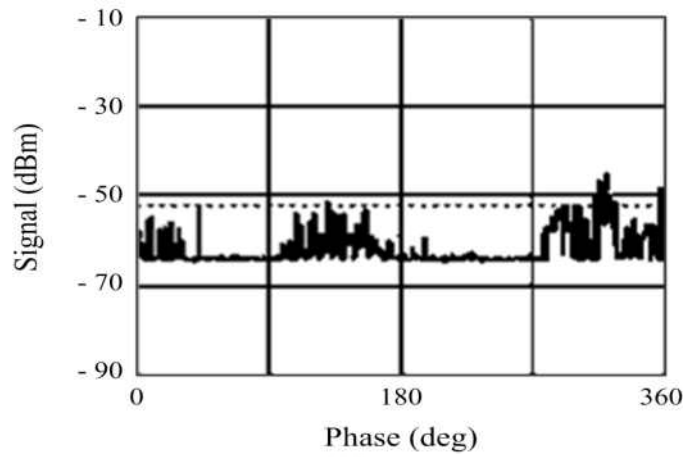
(b) Phase spectrum

Fig. 4.5 Frequency and phase spectrums measured in 170 kV GIS

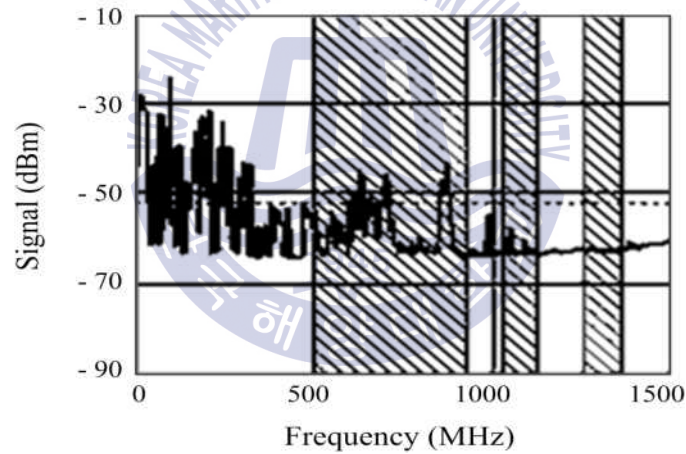Table 4.3 Diagnosis result of new method for 170 kV GIS

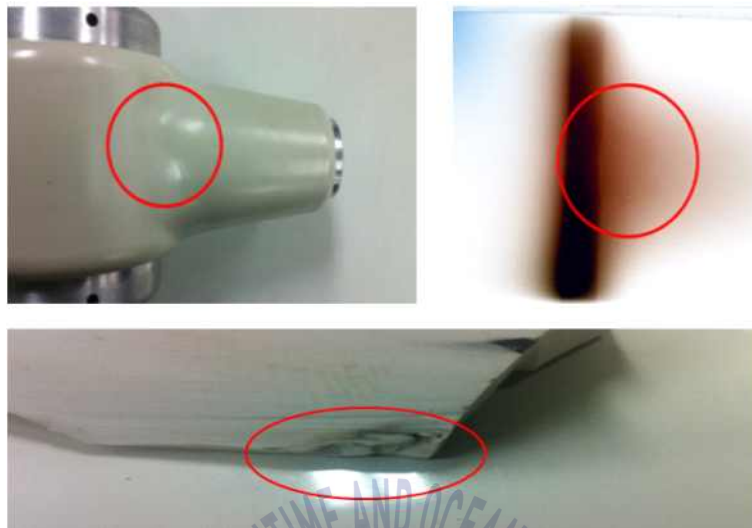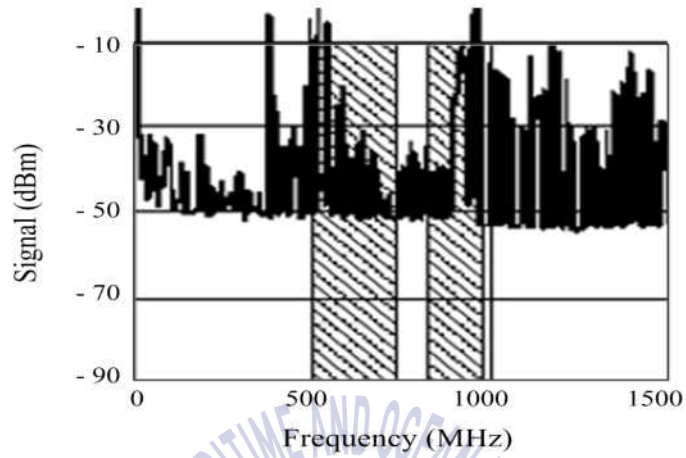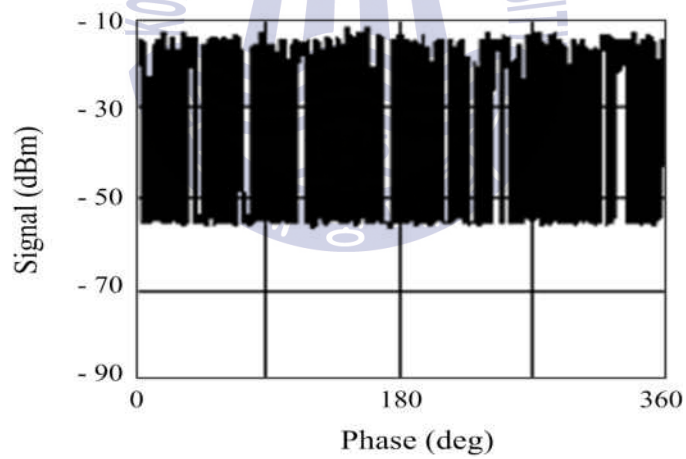| Diagnosis steps			New PD diagnostic algorithm
First step			Two groups
Second step	First group		Shape 3
	Second group		Shape 3
Third step	The number of distribution ranges		Two ranges
	Density levels	F1	High
		F2	Low
		F3	None
Fourth step	First peak		F1
	Second peak		F2
Diagnosis result			Void

Fig. 4.6 Photographs of internal defect in 170 kV GIS

c) Sensor connector fault case in Malaysia

An alarm had occurred in the 275 kV GIS of Malaysia on the on-line UHF PD device. The abnormal signal was detected by a few tens of UHF sensor installed on the GIS due to its high magnitude of nearly −10 dBm as shown in Fig. 4.7. The types of PD like floating or noise like external interference might had been presumed. The measured frequency and phase spectrum were analyzed with the conventional and new methods in the field. The on-site diagnosis results of conventional and new methods were the external noise and sensor connector fault, respectively. Table 4.4 shows the diagnosis result of new method for 275 kV GIS. From the result of the internal inspection by on-site engineers, it was found that the connector was not fixed inside the UHF sensor as shown in Fig. 4.8. After the new UHF sensor connector was replaced, the abnormal signal disappeared.

(a) Frequency spectrum

(b) Phase spectrum

Fig. 4.7 Frequency and phase spectrums measured in 275 kV GIS

Table 4.4 Diagnosis result of new method for 275 kV GIS

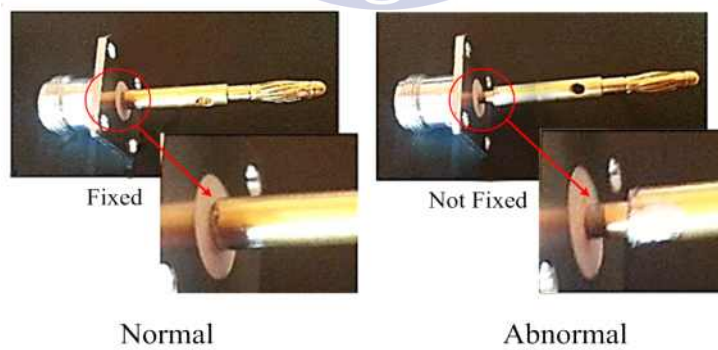| Diagnosis steps			New PD diagnostic algorithm
First step			One range
Second step	First group		Shape 10
	Second group		Shape 13
Third step	The number of distribution ranges		Full ranges
	Density levels	F1	High
		F2	High
		F3	High
Fourth step	First peak		F1
	Second peak		F3
Diagnosis result			Sensor connector fault

Fig. 4.8 Photographs of internal defect in 275 kV GIS

Chapter 5 Conclusions

This thesis described the phase-asynchronous PD diagnosis method for GISs. As mentioned in Chapter 3, the discharge phase is one of the most important parameters to identify and classify types of PD faults. In many cases of on-site PD measurement, however, the diagnosis results are not correct because most of the UHF PD measurements are performed without phase synchronization of voltage applied to in-service GIS. Therefore, the new method of PD diagnosis would be needed to identify and classify types of PD faults without phase synchronization for on-site PD measurement.

To develop the new method which can classify defect types using the phase-asynchronous PD patterns during on-site diagnosis, the 327 cases of on-site UHF PD data were collected from 2003 to 2015. The collected PD database were classified into 6 types of PDs and 4 types of noises. The statistical analysis of the UHF PD data were performed according to types of defects, types of PDs and noises, compartments and components, and voltage classes, and actions taken for inspections. The largest portion of defects was the PDs, and the most frequent PD and noise types were the floating elements and the external interferences, respectively. The most frequent GIS compartments and components in which PD occurred were the GIBs and the bolts. In case of voltage classes and actions taken for inspection, the PD occurred the most frequently in 362 kV GIS, and internal inspection and replacement work were performed the most frequently once a PD was detected.

To develop the new method of PD diagnosis which is applicable to the on-site PD diagnosis without phase synchronization, the features of frequency and phase parameters were extracted to classify defect types using the representative data of 82 cases including 66 PDs and 16 noises. The features consisted of 5 frequency parameters including the number of distribution ranges, maximum value, frequency ranges of first and second peak values, peak differences between first and second values, and density levels, and 6 phase parameters including the number of phase groups, overall distribution ranges or not, distribution ranges of each group, density levels, peak differences between the first and second groups, and shapes.

Depending on the criterions of 5 frequency and 6 phase parameters, 82 cases of the representative data were classified. The feature analysis was performed according to defects including types of 6 PDs and 4 noises. From the result, the 5 effective parameters were selected to classify types of 6 PDs and 4 noises clearly based on decision tree method, which included four steps; the number of groups in phase parameters, shapes in phase parameters, the number of distribution ranges & density levels in frequency parameters, and ranges of first and second peak value in frequency parameters. The first step using the number of phase groups was applied to distinguish the case of noise that could be classified less than 1 % of the total data. The second step using phase shapes was applied to distinguish the 32 cases of PDs and noises that could be classified about 40 % of the total data. The third step using frequency parameters combined with the number of distribution ranges & density levels was applied to distinguish the 49 cases of PDs and noises that could be classified about 42 % of the total data. Finally, the fourth step

using the frequency ranges of first and second peak values was applied to distinguished 9 cases of noises that could be classified about 11 % of the total data. To evaluate the new method for PD diagnosis proposed in this thesis, the diagnosis result was compared with that of the conventional method. The accuracy rate of conventional method was much less than that of the new method which was about 94% because the conventional method could not classify types of defects clearly using the phase-asynchronous PD data, which were caused by phase absence of voltage applied to GIS during on-site PD measurement.

The new method was also applied to on-site GIS diagnosis in South Korea and Malaysia to verify its reliability. In three cases, portable and on-line UHF PD systems were installed without phase synchronization, and the defect cause and location inside GISs were inspected visually by on-site engineers after on-site PD measurement. The three cases were analyzed by the new method based on decision-tree based diagnosis algorithm and diagnosis results of the new method were identical to results of internal inspection.

The new PD diagnosis method proposed in this thesis is quite useful to classify 6 types of PDs and 4 types of noises using the phase-asynchronous PD signals of GIS during the on-site diagnosis. It is a practical implement for non-expert maintenance managers to identify the type of defect and to make proper maintenance schedule. Furthermore, it could be expected to improve the reliability of diagnosis performance and to identify unresolved diagnosis area if additional representative data are collected in the future.

References

[1] U. Schichler, W. Koltunowicz, D. Gautschi, A. Girodet, H. Hama, K. Juhre, J. Lopez-Roldan, S. Okabe, S. Neuhold, C. Neumann, J. Pearson, R. Pietsch, U. Riechert and S. Tenbohlen, "UHF Partial Discharge Detection System for GIS: Application Guide for Sensitivity Verification", IEEE Trans. Dielectr. Electr. Insul., Vol. 23, No. 3, pp. 1313-1321, 2016.

[2] Hyang-Eun Jo, Guoming Wang, Sun-Jae Kim and Gyung-Suk Kil, "Comparision of Partial Discharge Characteristics in SF6 Gas Under AC and DC", Trans. Electr. Electron. Mater., Vol. 16, No. 6, pp. 323-327, 2015.

[3] CIGRE WG A3.06, "Final Report of the 2004-2007 International Enquiry on Reliability of High Voltage Equipment", CIGRE Technical Brochure No. 513, 2012.

[4] S. M. Neuhold, "On site tests of GIS", Highvolt Kolloquium, 2011.

[5] IEC 60071-2, "Insulation coordination-Part 2: Application Guide", 1996.

[6] Guo, H., Lu, F., and Ren, K. F., "Simulation and Measurement of PD-induced Electromagnetic Wave Leakage in GIS with Metal Belt", IEEE Trans. Dielectr. Electr. Insul., Vol. 21, No. 4, pp. 1942-1949, 2014.

[7] Mizuno, K., Ogawa, A., Nojima, K., Murase, H., Koyama, H., and Wakabayashi, S., "Investigation of PD Pulse Propagation Characteristics in GIS", IEEE Trans. Power Syst., Vol. 12, No. 2, pp. 1022-1030, 1997.

[8] Metwally, I. A., "Status Review on Partial Discharge Measurement Techniques in Gas-insulated Switchgear/Lines", Electr. Power Syst. Res.,

Vol. 69, No. 1, pp. 25-36, 2004.

[9] Kamei, M., and Takai, O., "Influence of Sensor Information Accuracy on Condition-Based Maintenance Strategy for GIS/GCB Maintenance", IEEE Trans. Pow. Deliv., Vol. 26, No. 2, pp. 625-631, 2001.

[10] IEC Publication 60270, High-voltage test techniques: Partial discharge measurements, 2000.

[11] CIGRE WG D1.03, "Risk Assessment on Defects in GIS Based on PD Diagnostics", CIGRE Technical Brochure No. 525, 2013

[12] CIGRE JWG 33/23.12, "Insulation Co-ordination of GIS: Return of Experience, On Site Tests and Diagnostic Techniques", Electra No. 176, 1998.

[13] M. Pompili, C. Mazzetti, and R. Bartnikas, "Simultaneous ultrawide and narrowband dectection of PD pulses in dielectric liquids", IEEE Trans. Dielectr. Electr. Insul., Vol. 5, No. 3, pp. 402-407, 1998.

[14] CIGRE WG 23.10, "Report on the second international survey on high voltage gas insulated substations(GIS) service experience", pp. 23-102, 1998.

[15] H. Ma, J. C. Chan, T. K. Saha, and C. Ekanayake, "Pattern recognition techniques and their applications for automatic classification of artificial partial discharge sources", IEEE Trans. Dielectr. Electr. Insul., Vol. 20, No. 2, pp. 468-478, 2013.

[16] CIGRE WG, "Long-Term Performance of SF6 Insulated Systems", 2002.

[17] M. Wu, H. Cao, J. Cao, H. L. Nguyen, J. B. Gomes, and S. P. Krishnaswamy, "An overview of state-of-the-art partial discharge analysis techniques for condition monitoring", IEEE Electr. Insul. Mag., Vol. 31,

No. 6, pp. 22-35, 2015.

[18] H. E. Jo, G. M. Wang, S. J. Kim, and G. S. Kil, "Comparison of partial discharge characteristics in SF6 gas under AC and DC", Trans. Electr. Electron. Mater., Vol. 16, No. 6, pp. 323-327, 2015.

[19] CIGRE WG D1.33, "Guide for Partial Discharge Measurements in Compliance to IEC 60270", CIGRE Tech. Broch. No. 366, 2008.

[20] Sacha M. Markalous, Stefan Tenbohlen, Kurt Feser, "Detection and Location of Partial Discharges in Power Transformers using Acoustic and Electromagnetic Signals", IEEE Trans. Dielectr. Electr. Insul., Vol. 15, pp. 1,576-1,583, 2008.

[21] N. Giao Trinh, "Short Notes on the Physics of Corona Discharge", IEEE/PES Special Course on Corona and Field Effects of High Voltage Transmission Lines, 1981.

[22] R. Davis, M. Frearson, "Mass Spectrometry-Analytical Chemistry by Open Learning", John Wiley & Sons, 1987.

[23] F. H. Kreuger, "Partial Discharge Detection in High Voltage Equipment", Butterworth, pp. 129-152, 1989.

[24] 趙智大, "高電壓技術", 中國電力出版社, pp. 83-87, 2006.

[25] CIGRE WG D1.25, "UHF Partial Discharge Detection System for GIS : Application Guide for Sensitivity Verification", CIGRE Tech. Broch. No. 654, 2016.

[26] Riechert, Linn, Winkler, Pietsch, "Reasonable Application of UHF-Partial Discharge Measurements in Development, Production and Service of Gas Insulated Switchgear(GIS)", CIGRE SC 15 Symposium, Dubai, United Arabic Emirates, 2001.

[27] CIGRE WG D1.37, "Guidelines for Partial Discharge Detection using Conventional (IEC60270) and Unconventional Methods", CIGRE Tech. Broch. No. 662, 2016.

[28] S. Meijer, R. G. A. Zoetmulder, J. J. Smit, "Risk Assessment of Free Moving Particles in GIS using Spectral and Partial Discharge Analysis", IEEE Inter. Symp. Elect. Insul., Boston, 2016.

[29] CIGRE WG 15.03, "Diagnostic Methods for GIS Insulating Systems", CIGRE Session, CIGRE Report 15/23-01. 15/23-01, 1992.

[30] C. M. Cooke, R. E. Wootton, A. H. Cookson, "Influence of Particles on AC and DC Electrical Performance of Gas Insulated Systems at Extra-High-Voltage", IEEE Trans. Pow. App. Syst., Vol. PAS-96, No. 3, pp. 768-777, 1977.

[31] B. Qi, C. Li, Z. Xing, Z. Wei, "Partial Discharge Initiated by Free Moving Metallic Particles on GIS Insulator Surface: Severity Diagnosis and Assessment", IEEE Trans. Dielectr. Electr. Insul., Vol. 21, No. 2, pp. 766-773, 2014.

[32] R. Baumgartner, B. Fruth, W. Lanz, K. Pettersson, "Partial Discharge-Part IX: PD in Gas-Insulated Substations – Fundamental considerations", IEEE Elect. Insul. Mag., Vol. 7, No. 6, 1991.

[33] L. Niemeyer, "A generalized approach to partial discharge modeling", IEEE Trans. Electr. Insul. Vol. 2, No. 4, pp. 510-525, 1995.

[34] S. A. Boggs, "Partial Discharge Part III: Cavity-Induced PD in Solid Dielectrics", IEEE E.I.M., Vol. 6, No. 6, pp. 11-16, 1990.

[35] Cavallini, F. Ciani, G. Mazzanti, G.C. Montanari, "First Electron Availability and Partial Discharge Generation in Insulation Cavities: Effect

of Light Irradiation", IEEE Trans. Electr. Insul. Vol. 12, No. 2, pp. 387-394, 2005.

[36] IEC 62271-203, "High-voltage switchgear and controlgear-Part 203: Gas-insulated metal-enclosed switchgear for rated voltages above 52kV", 2001.

[37] Hampton, Meats, Pryor, Watson-Jones, "The Application of Partial Discharge Measurements to GIS", Intern. Symp., pp. 313-321, 1985.

[38] L.E. Lundgaard, "Particles in GIS: Behaviour and Possibilities for Characterisation from Acoustic Signatures", IEEE Trans. Electr. Insul., Vol. 8, No. 6, pp. 1064-1074, 2001.

[39] CIGRE WG D1.33, "High-voltage On-site Testing with Partial Discharge Measurement", CIGRE Tech. Broch. 502, 2012.

[40] CIGRE WG 15.03, "Effective of Particles on GIS and the Evaluation of Relevant Diagnostic Tools", CIGRE Session, CIGRE Report 15-103, 1992.

[41] CIGRE WG D1.33, "Guidelines for Unconventional Partial Discharge Measurements", CIGRE Tech. Broch. 444, 2010.

[42] A. Bargigia, W. Koltunowicz and A. Pigini, "Detection of Partial Discharges in Gas Insulated Substations", IEEE Trans. Pow. Deliv., Vol. 7, No. 3, pp. 1239-1249, 1992.

[43] CIGRE WG B3.24, "Benefits of PD diagnosis on GIS condition assessment", CIGRE Tech. Broch. 674, 2017.

[44] B. Hampton, R. Meats, "Diagnostic Measurements at UHF in Gas Insulated Substations", IEEE Proceeding C: Generation, Transmission and Distribution, Vol. 135, No. 2, pp. 137-145, 1988.

[45] J. Pearson, O. Farish, B. Hampton, M. 4Judd, D. Templeton, B. Pryor, I. Welch, "Partial Discharge Diagnostics for Gas Insulated Substations", IEEE Trans. Dielectr. Electr. Insul., Vol. 2, No. 5, 1995.

[46] M. Judd, O. Farish, B. Hampton, "The Excitation of UHF Signals by Partial Discharges in GIS", IEEE Trans. Dielectr. Electr. Insul., Vol. 3, pp. 213-228, 1996.

[47] IEC 62478, "High-voltage test techniques: Measurement of partial discharge by electromagnetic and acoustic methods", 2001.

[48] Masayuki, Ohtsuka, Ueta, Okabe, Hoshino, Maruyama, "Influence of Insulating Spacer Type on Propagation Properties of PD-induced Electromagnetic Wave in GIS", IEEE Trans. Dielecr. Electr. Insul., Vol. 17, No. 5, 2010.

[49] Masayuki, Ohtsuka, Teshima, Okabe, Kaneko, "Examination of Electromagnetic Mode Propagation Characteristics in Straight and L-Section GIS Model using FD-TD Analysis", IEEE Trans. Dielecr. Electr. Insul., Vol. 14, No. 6, 2007.

[50] Okabe, Kaneko, Yoshimura, Muto, Nishida, Kamei, "Partial Discharge Diagnosis Method using Electromagnetic Wave Mode Transformation in Gas Insulated Switchgear", IEEE Trans. Dielecr. Electr. Insul., Vol. 14, No. 3, 2007.

[51] CIGRE TF 15/33.03.05, "PD Detection System for GIS: Sensitivity Verification for the UHF Method and the Acoustic Method", Electr. No. 183, 1999.

[52] L. Lundgaard, "Partial Discharge - Part XIII: Acoustic Partial Discharge Detection-Fundamental Considerations", IEEE Electr. Insul. Mag., Vol. 8,

No. 4, 1992.

[53] L. Lundgaard, "Partial Discharge-Part XIV: Practical Application", IEEE Electr. Insul. Mag., Vol. 8, No. 5, 1992.

[54] L. Lundgaard, B. Skyberg, A. Schei, A. Diessner, "Method and instrumentation for acoustic diagnoses of GIS", CIGRE session, pp. 15-309, 2000.

[55] Lapp, A., Kranz, H.-G., "The use of the CIGRE data format for PD diagnosis applications", IEEE Trans. Dielecr. Electr. Insul., Vol. 7, No. 1, pp. 102-112, 2000.

[56] R. Bozzo, L. Centurioni, F. Guastavino, "Measuring the Endurance of Films in Partial Discharges", IEEE Trans. Dielecr. Electr. Insul., Vol. 28, No. 6, pp. 1050-1056, 1993.

[57] Rolnad Piccin, "Partial Discharge Analysis in HVDC Gas Insulation Substations", Ph.D Thesis, Delft Univ. Tech., 2013.

[58] T. Kato, F. Endo, S. Hironaka, "Sensitivity Calibration of UHF Partial Discharge Monitoring System in GIS", IEE of Japan, Vol. 122-B, No. 11, 2002.

[59] J. Y. Koo, S. Y. Jung, C. H. Ryu, S. W. Lee, B. W. Lee, "Identification of insulation defects in gas-insulated switchgear by chaotic analysis of partial discharge", IET Science, Meas. Tech. Vol. 4, No. 3. pp. 115-124, 2010.

[60] Korea Electric Power Corporation, Electric Power Research Institute, "Investigation of GIS partial discharge detection technology", Final report, Electric Power Research : Cooperative 413, 2002.

Acknowledgements

My deep gratitude goes first and foremost to my supervisor, Prof. Gyung-Suk Kil, for his inspired guidance, valuable comments, insightful criticism, great patience, constant encouragement and support throughout the entire period of my research study. His enthusiasm, rigorous attitude and dedication to scientific research are strongly impressed on my memory. His expert advices greatly help me improve the depth of my research. The profound and invaluable knowledge that I gained from him will benefit me in my future life and career.

I would like to acknowledge helpful suggestions from my committee members: Prof. Yoon-Sik Kim, Prof. Nak-Won Jang, Dr. Heung-Gi Cho, and Dr. Young-Jin Cho. I am also thankful to Prof. Sung-Geun Lee, Prof. Tae-In Jeon, Prof. Dong-Hoan Seo, and Prof. Yang-Ick Joo for their kind gudiance and insightful comments on my thesis.

I wish to express my sincere thanks to Mr. Seung-Yong Park, Head of R&D Center, Hyosung Corporation, for approving the PhD course. I am very thankful to members of Power Asset Management(PAM) team : Mr. Jae-Ryong Jung, Mr. Hwang-Dong Seo, Mr. Young-Min Kim, Mr. Eun-Tae Lyu, Mr. Sung-Jik Kim, and Dr. Hyang-Eun, for their help and co-operation in completing my thesis successfully. I am highly grateful to Ms. Yun-Hee Jeong, Research Management Team, for her invaluable support.

I would like to acknowledge the valuable help from all members in Applied High Voltage Laboratory for their help and understanding. I convey